Environmental Earth Sciences (2024) 83:523
https://doi.org/10.1007/s12665-024-11811-y

ORIGINAL ARTICLE

Petrogaphic and structural analyses of high-grade amphibolites from Fotouni-Kékem and Nyakong-Manyi shear zones: implications for the geodynamic significance of the Central Cameroon Shear Zone

Tcheumenak Kouémo Jules[1] · Sobze Yemdji Belmien Robinson[2] · Fozing Eric Martial[2] · Tepi Yemele Brice Rostant[2] · Azefack Mbounou Rodolph Loïque[2] · Kwékam Maurice[2,3]

Received: 28 October 2023 / Accepted: 10 August 2024 / Published online: 30 August 2024

Abstract

Fotouni-Kékem shear zone (FKSZ) and the Nyakong-Manyi shear zone (NMSZ) are respectively located to southwest and northwest of the N50E branch of the central Cameroon shear zone (CCSZ). Three deformation phases are recorded in these shear zones including, D_1, D_2 and D_3. The D_1 phase, with σ_1 applied in the NE-SW direction, is remnant and poorly represented, whose structures (NW–SE S_1 foliation) were transposed by the late D_2 and D_3 phases related structures. The D_2 phase is an early sinistral shear phase, with σ_1 applied in the WNW-ESE direction, which developed NNW-SSE to NNE-SSW S_2 foliation, B_2 shear band boudins, F_2 knee-like folds and asymmetric fish-like structures. The D_3 phase is a NE-SW dextral mylonitic shear phase, with σ_1 applied in the NW–SE direction, responsible the development of S_3 foliation, P_3 recumbent and overturn folds, B_3 shear band boudins, σ-type sigmoids and asymmetric amphibole fishes. Pyroxene amphibolite (PA) occurs as slab stones, banded to lens-like, egg-like enclaves, folded bands, sheared and/or boudinaged green to dark green rocks displaying NE-SW preferred orientation. It displays heterogranular nematoblastic texture marked by amphibole (60%, hornblende), plagioclase (≈20%) and clinopyroxene (15 à 20%) porphyroblasts dispersed in between medium-grained mineral showing preferred orientation. Under microscope, PA evidenced a polyphasic prograde-peak-retrograde high-grade regional metamorphism. Prograde-peak phase is evidenced by primary mineral paragenesis (stable amphibole + pyroxene + plagioclase + K-feldspar) and microstructures, which indicate granulite facies. This occurs during the D_1 deformation phase. retromorphic relic-like pyroxene crystals displaying amphibole-plagioclase-quartz-opaque minerals assemblage, which follows the peak metamorphism, related to relaxation during D_2-D_3, evidence retrograde phase. Early sinistral syn-D_2 and late dextral syn-D_3 mylonitic events, whose microstructures evidence high-grade deformation setting, overprinted this regional metamorphism. This polyphasic activation of the CCSZ during these mylonitic events (D_2-D_3) stretched, sheared, folded dismembered and scattered amphibolites along the Pan-African mobile zone during late phases of the Pan-African orogeny. Geochemical data indicate that PA derives from mafic protoliths originating from a garnet lherzolite reservoir melting that was contaminated by both subducted sediment and slab-derived fluids as evidenced by the slightly positive εNd_{600Ma} (+ 1.27). The model age (T_{DM} = 1.25 Ga) with initial $^{87}Sr/^{86}Sr$ ratios of 0.70488 suggest an ancient Mesoproterozoic crust that underwent metamorphic transformation during the collisional (burial) and post collisional (exhumation) stapes of the Pan-African orogeny.

✉ Tcheumenak Kouémo Jules
tcheumenak2@gmail.com; jtcheumenak@fs-univ-douala.cm

[1] Department of Earth Sciences, Faculty of Science, University of Douala, P.O. Box 24157, Douala, Cameroon

[2] Department of Earth Sciences, Faculty of Sciences, University of Dschang, P.O. Box 67, Dschang, Cameroon

[3] Geowissenschaftliches Zentrum Göttingen, Georg-August-Universität Göttingen, Goldschmidt-Straße 1, 37077 Göttingen, Germany

Keywords High-grade pyroxene amphibolites · Fotouni-Kékem and Nyakong-Manyi shear zones · Prograde-peak-retrograde metamorphism · Pyroxene retrograde microstructures · Gabbroic protoliths · Mesoproterozoic crust

Introduction

High-grade metamorphic rocks are described in the Central African Fold Belt (CAFB, Fig. 1a). There are mostly described in metapelitic gneiss and mylonites (which are much more abundant than amphibolites) and usually occur as highly strained elongated rock bodies, bands or small lenses interbedded with migmatites in the central and southern Cameroon domains (Bouyo Houkentchang et al. 2009, 2013; Efon Awoum et al. 2020; Tcheumenak Kouémo et al. 2023; Sobze Yemdji et al. 2023). Green rocks like amphibolites are actually recorded in subduction settings and orogenic belts thus constituting good example of environment for the formation of this particular rock type (Ganwa 2005; Fozing et al. 2019). Moreover, numerous interpretations and geodynamic models have been proposed to explain the formation of like amphibolites, including their significance as geological evidences of: (i) insular arcs in an active margin setting (Condie 1997; De Wit 1998), (ii) intra-continental rifts (Hunter et al. 1998) or (iii) orogenic belts (Ganwa 2005; Fozing et al. 2019; Bouyo Houketchang et al. 2013). Very little is unfortunately known about amphibolites of the CAFB and the Pan-African history in general and Pan-African metamorphism in particular. The scarcity, the mode of outcrop as small enclaves and the limited exposure extensions of these amphibolites may probably be explained by the fact that, they are rarely used for pressure–temperature (*P*–*T*) metamorphic and geodynamic reconstructions of the CAFB. They generally occurs as small centimetric- to metric-size enclaves scattered throughout the central and northern Cameroon domain but poorly studied up to now except some few studies (Ganwa 2005; Fozing et al. 2019; Njanko et al. 2012; Bouyo Houkentchang et al. 2013). However lens-like as well as shear and boudinaged amphibolites bodies, in addition to egg-like enclaves are well recorded in kyanite-sillimanite-garnet gneisses in both the Fotouni-Kékem shear zone (FKSZ) and the Nyakong-Manyi shear zone (NMSZ). The FKSZ and the NMSZ consist of the same rock types including pyroxene amphibolites and kyanite-sillimanite-garnet gneisses, except for the charnockites that outcrops only in the FKSZ. The occurrence of these scarce pyroxene amphibolites displaying various shapes in the FKSZ and NMSZ along the central Cameroon shear zone (CCSZ, the most characteristic megatectonic feature of the central domain of the CAFB in Cameroon), may help in understanding their history with respect to the lithotectonic evolution of the CCSZ and CAFB. In addition, according to some few research works (Efon Awoum et al. 2020; Tcheumenak Kouémo et al. 2023; Sobze Yemdji et al. 2023), high-grade metamorphism is evoked for the studied amphibolites although the aforementioned research works are not focused on these green rocks. Also, very little is known about the geochemical and the Sr–Nd significances of these rocks.

Based on petrographic, microstructural, geochemical (whole-rock and Sr–Nd) data of amphibolites from FKSZ and NMSZ, this paper aims to: (i) contribute to clarify its structural evolution with respect to the CCSZ history; (ii) characterize their origin; (iii) estimate their pressure–temperature-time (*P*–*T*-*t*) path evolution and (iv) explain the significance of their elongated- and dismembered-like distributed throughout the central and northern domains of the CAFB. It also discusses their significance for the better understanding of the geodynamic evolution of the CAFB during the Pan-African orogeny.

Geological setting

The Central African Fold Belt (CAFB)

The CAFB in Cameroon (Fig. 1a; Penaye et al. 1993; Toteu et al. 2001) is a remobilized geolological megastructure limited to the north by the Saharan Metacraton and to the south by the Congo Craton (Abdelsalam et al. 2002; Liégeois et al. 2013). It is organized into three lithostructural domains: the northern, central and southern domains (Fig. 1b).

The Sanaga Fault, also known as the Sanaga shear zone (SSZ) and to the north by the Tcholliré-Banyo Fault (Toteu et al. 2004; Njanko et al. 2006), borders the central domain to which belongs the study areas to the south. The Central Cameroon Shear Zone (CCSZ, (Figs. 1b, 2) is the most characteristic megastructure of the central domain. It displays mega thrust zones and is associated mylonitic corridors, which result from ductile post-collisional deformation (Toteu et al. 2004; Ngako et al. 2003, 2008; Njanko et al. 2006, 2010; Njonfang et al. 2006, 2008; Efon Awoum et al. 2020; Tcheumenak Kouémo et al. 2023; Sobze Yemdji et al. 2023). Three deformation phases (D_1, D_2 and D_3) are recorded in the central domain. The D_1 (613–590 Ma, zircon U–Pb method, Kwékam et al. 2010) is a flattening phase marked by NW–SE to NNE-SSW foliations and high-grade metamorphism (Tchaptchet Tchato et al. 2009; Bouyo Houkentchang et al. 2013; Tcheumenak Kouémo et al. 2023).

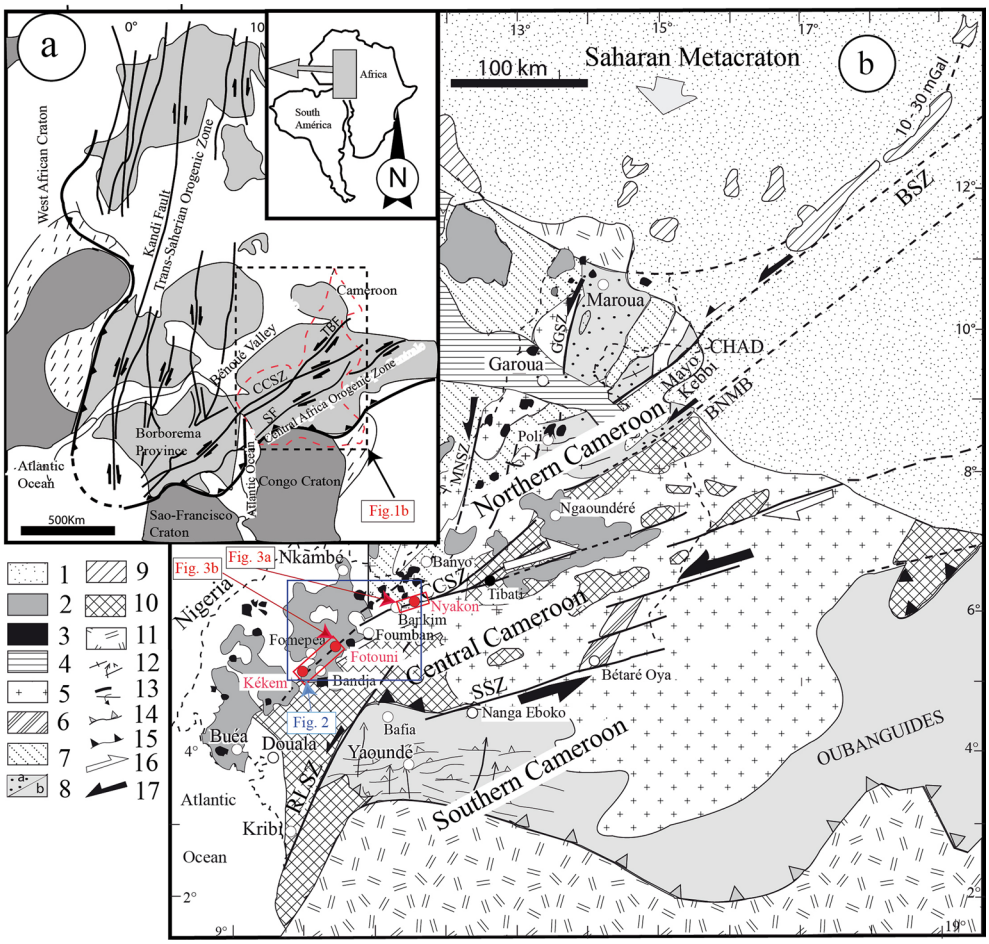

Fig. 1 **a** Pan-African shear zone network in a pre-Mesozoic reconstruction (After Caby et al. 1991). Structural map of Cameroon showing the study area. **b** Structural map of Cameroon (After Toteu et al. 2001, Ngako et al. 2008 and Njanko et al. 2010). 1: Quaternary sediments; 2: Cameroon Volcanic Line; 3: Cameroon plutonic line; 4: Mesozoic sediments (Benue Trough); 5: Late- to syn-tectonic subalkaline granitoids (meta-sediments, conglomerates, volcanic ashes, and lavas); 6: Lom syn-tectonic basin; 7: West Cameroon Domain Domain (WCD; early syn-tectonic basic to intermediate calc-alkaline intrusions, 660–600 Ma); 8a: Poli Group (active margin Neoproterozoic supracrustal); 8b: Yaoundé Group (intracratonic deposits and juvenile intrusions); 9: Massenya-Ounianga high gravities (10–30 mGal); 10: Adamawa-Yadé and Nyong Paleoproterozoic Remnants; 11: Craton and inferred craton; 12: *S*2 foliation and *L*2 lineation trends; 13: *F*2 upright and overturned antiforms; 14: Syn-*D*2 main frontal thrust zone; 15: Syn-*D*1 thrust zone (separates the LP to MP zone in the North from the HP zone in the South); 16: Syn-*D*3 sense of shear movement; 17: Syn-*D*2 sense of shear movement. Large gray arrow represents syn-*D*1–3 regional main stress direction. Thick lines = shear zone (SZ): BSZ = Baché SZ; BNMB = Buffle Noir- Mayo Baleo SZ; CCSZ = Central Cameroon SZ; GGSZ = Godé-Gormaya SZ; MNSZ = Mayo Nolti SZ; RLSZ = Rocher du Loup SZ; SSZ = Sanaga SZ

The D_2 (590–576 Ma, zircon U–Pb method; Kwékam et al. 2010, 2013) is a transcurrent sinistral deformation phase, which is responsible for the development of (i) NNE-SSZ to NE-SW mylonitic corridors, (ii) pull-apart structures and the emplacement of Syn-D_2 plutonic intrusions (e.g. the Fomopéa, Bandja, Batié, Dschang, Santchou, Ndiéki, Ngondo and Ngwi granitic plutons) parallel to regional structures' trend (Nguiessi Tchamkam et al. 1997; Tagne-Kamga et al. 1999; Kwékam et al. 2010; Tcheumenak Kouémo et al. 2014, 2023; Efon Awoum et al. 2020; Achu Megnemo et al. 2021; Fozing et al. 2021; Kamgang Tchuifong et al. 2022). D_3 phase (576–542 Ma, zircon U–Pb method by Kwékam et al. 2010, 2013 and EPMA-Th-U–Pb monazite method by Tchaptchet Tchato et al. 2009) is a NE-SW dextral shear deformation phase characterized by an intense mylonitization, that strongly deformed the para- and ortho- gneisses (Njonfang et al. 2008; Njanko et al. 2010; Tcheumenak Kouémo et al. 2014, 2023; Efon Awoum et al. 2020; Fozing et al. 2021; Kamgang Tchuifong et al. 2022; Sobze Yemdji et al. 2023).

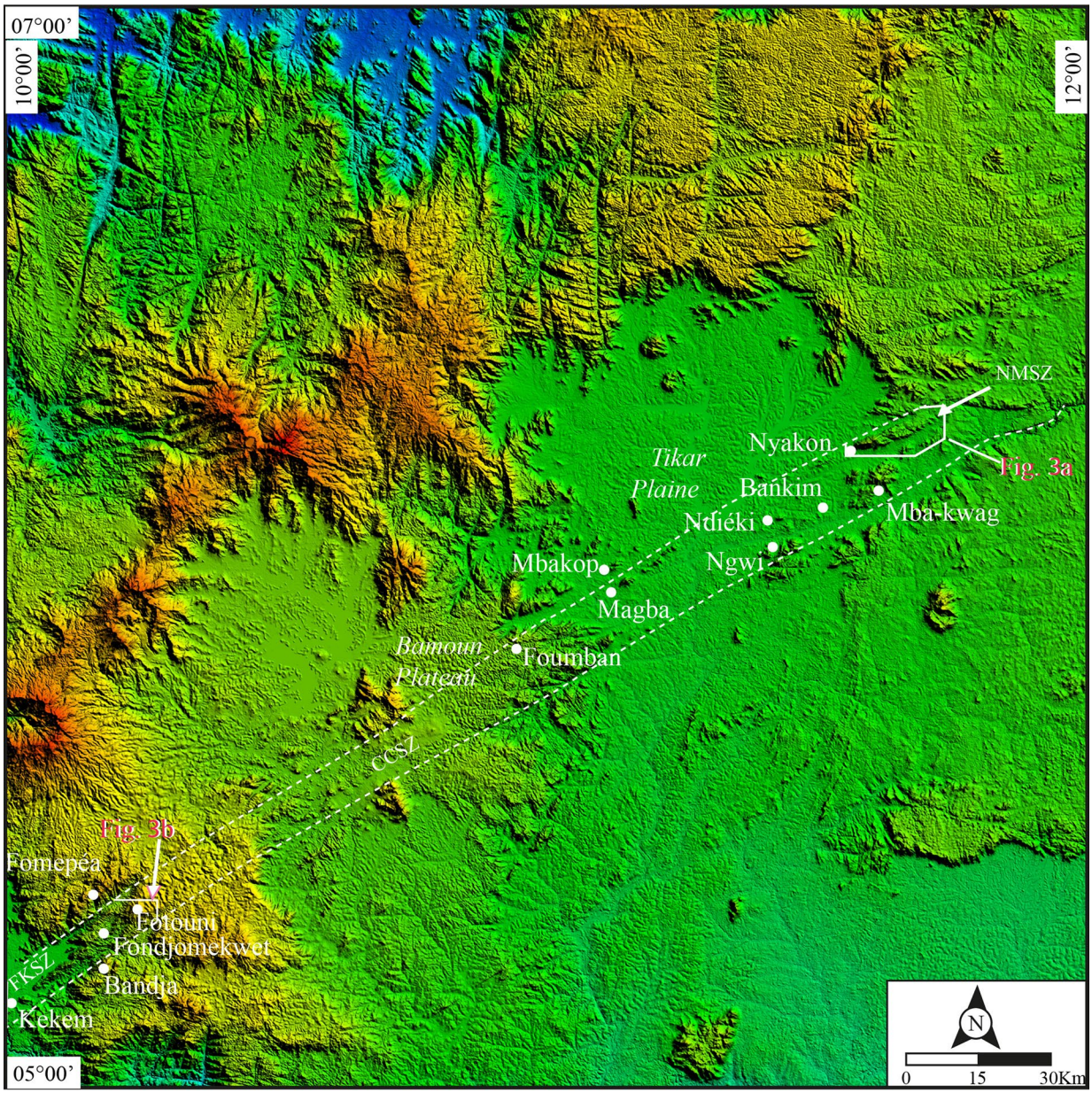

Fig. 2 SRTM image showing the study areas, the CCSZ and its different studied segments including the FKSZ and the NMSZ

Central Cameroon shear zone (CCSZ)

The CCSZ displays two trends: a (i) N70E trend for the Tibati branch and a (ii) N30E-N50E trend for the Nyakong-Kékem branch (Figs. 1b, 2). Mylonites are recorded in the Fotouni-Kékem (Tcheumenak Kouémo et al. 2014, 2023; Tchaptche Tchato et al. 2009) in the Foumban-Bankim (Njonfang et al. 2006, 2008; Efon Awoum et al. 2020) and the Nyakong-Manyi (Sobze Yemdji et al. 2023) areas. Along the CCSZ corridor, granulitic rocks occur as discontinuous or remnant rock bodies (mostly paragneisses), lenses or bands dismembered, sometimes mylonitized and scattered by either Pan-African granitoids or by the shear zones (Penaye et al. 1993; 2004; Toteu et al. 2001; Tchaptchet Tchato et al. 2009; Bouyo Houkentchang et al. 2009; Tcheumenak Kouémo et al. 2014, 2023; Tchaptchet Tchato et al. 2009). These rock bodies are mostly pelitic, metamorphosed in granulite facies (Tchaptchet Tchato et al. 2009; Bouyo Houkentchang et al. 2009; 2013; Tcheumenak Kouémo et al. 2023) displaying garnet-kyanite-K-feldspar-biotite metapelites. Some few metabasites are described in the Banyo area (located to the NE of the study area) by Bouyo Houkentchang et al. (2009, 2013). They include high-grade metamorphic rocks of basic to intermediate composition occurring as

very small lenses or units of garnet pyroxenites that are generally adjacent to pelitic gneisses in the field (Bouyo Houkentchang et al. 2009, 2013; Ganwa 2005). The most common characteristic features of these metabasites are (i) the development of migmatitic features and (ii) the presence of orthopyroxene displaying corona texture or symplectic porphyroblasts (Bouyo Houkentchang et al. 2013). According to Bouyo Houkentchang et al. (2013) the garnet-clinopyroxene-quartz, garnet-orthopyroxene-plagioclase, garnet-clinopyroxene-plagioclase, garnet-clinopyroxene-orthopyroxene-plagioclase ± hornblende assemblages are indicative of peak metamorphism P–T at 8-11kbar/730–780 °C. These high-grade metabasites are strongly affected by retrograde metamorphism marked by the abundance of symplectite and corona textures, as well as hydration reactions. These petrographic features according to Bouyo Houkentchang et al. (2013), correspond to isothermal decompression path.

In the Central Cameroon domain, the CCSZ represents one of the most characteristic megastructures. It strikes N70°E for the Tibati branch and curves at N30E-N50E for the Kékem-Nyakon branch (Njonfang et al. 2006; 2008; Njanko et al. 2006, 2010; Efon Awoum et al. 2020; Achu Megnemo et al. 2021; Kamgang Tchuifong et al. 2022; Tcheumenak Kouémo et al. 2014, 2023; Sobze Yemdji et al. 2023). The CCSZ displays complex kinematic evolution evidenced by approximate same direction multi-shear phases and multi-phase foliations which transposed D_1-related features during the sinistral shear phase (D_2) and itself later transposed during the D_3 dextral shear phase as evidenced by atypic complexes δ-type sigmoids (Ngako et al. 2003, 2008; Njonfang et al. 2008; Kwékam et al. 2010; Tcheumenak Kouémo et al. 2014; 2023; Bella Nké et al. 2018; Efon Awoum et al. 2020; Sobze Yemdji et al. 2023). The D_1 phase displays NW–SE foliation (S_1) that occurs as remnant structures in para- and ortho gneisses (Efon Awoum et al. 2020; Achu Megnemo et al. 2021; Sobze Yemdji et al. 2023). The D_2 phase displays N-S to NNE-SSW structures, associated N30E-N50E aligned and elongated series of hills trends which are parallel to the CCSZ' N30E-N50E branch (Njonfang et al. 2008; Kwékam et al. 2010, 2015, 2020a, b; Tcheumenack Kouémo et al. 2014; 2023; Efon Awoum et al. 2020; Achu Megnemo et al. 2021; Sobze Yemdji et al. 2023). The D_3 phase is a dextral NE-SW shear phase represented by numerous structural features like the mylonitic and metamorphic foliations, δ- and σ- type sigmoids (Njonfang et al. 2008; Sobze Yemdji et al. 2023).

Geology of the Fotouni-Kékem and Nyakong-Manyi shear zones

The Nyakong-Manyi shear zone (NMSZ) and Fotouni-Kékem shear zone (FKSZ) are NE-SW corridors respectively located to the northwest and the southwest of the N30E-N50E branch of the CCSZ. Controversial chronologic models have been proposed for the kinematic evolution of the sinistral and dextral shear phases in the FBSZ including: (i) early dextral and late sinistral shear phases for some authors like Ntiechie et al. (2017) and Efon Awoum et al. (2020) and (ii) early sinistral and late dextral shear for others like Njonfang et al. (2008), Bella Nké et al. (2018), Achu Megnemo et al. (2021) and Sobze Yemdji et al. (2023). The early sinistral (610–580 Ma, Ngako et al. 2003; 2008) and late dextral (585–540 Ma, Ngako et al. 2003, 2008) model is, in accordance to research works from Tcheumenak Kouémo et al. (2014, 2023) in the Fotouni-Kékem shear zone. Structural field and microstructural data from both the FKSZ and NMSZ evidenced three deformation phases (D_1, D_2 and D_3). The D_1 phase (613–600 Ma, zircon U–Pb method, Kwékam et al. 2010) is a NE-SW trending flattening phase whose main stress σ_1 developed NW–SE foliation (S_1) occurring as remnant structures in para- and ortho- gneisses (Efon Awoum et al. 2020; Achu Megnemo et al. 2021; Sobze Yemdji et al. 2023). It displays low to moderate dips (15–45°) with the mineral paragenesis consisting of garnet + kyanite + sillimanite, which experienced transposition during the D_2 phase. D_2 phase (613–590 Ma, EPMA-Th-U–Pb monazite method (Tchaptchet Tchato et al. 2009) and U–Pb method (Kwékam et al. 2010)) is a sinistral N-S to NNE-SSW shear phase characterized by S_2 metamorphic and mylonitic foliations, B_2 boudins, F_2 fold axes and L_2 stretching mineral lineation (Tcheumenak Kouémo et al. 2023; Sobze Yemdji et al. 2023). D_3 (590–542 Ma, EPMA-Th-U–Pb monazite method (Tchaptchet Tchato et al. 2009) and U–Pb method (Kwékam et al. 2010) is a NE-SW dextral shear phase characterized by ductile clockwise C_3 shear planes, F_3 folds and B_3 boudins.

From a lithological point of view, the FKSZ and NMSZ consist of the same rock types including protomylonites, amphibolites and kyanite-sillimanite-garnet mylonites and ultramylonites, kyanite-sillimanite-garnet gneisses, pyroxene amphibolites, and migmatites except for the charnockites, which outcrops only in the FKSZ (Fig. 3a–b). Garnet-sillimanite-kyanite gneiss (paragneiss) crops out as foliated slab stones on hillslopes and hilltops, and along road trenches or as rock pockets within ultramylonites in the FKSZ. It consists of quartz, K-feldspar, plagioclase, biotite, garnet, sillimanite, kyanite, opaque minerals, and zircon. Amphibolites outcrop as slab stones, boudinaged or folded rocks in garnet-kyanite-sillimanite ultramylonites and in protomylonites or as restites in migmitites, in theses shear zones (FKSZ and NMSZ). They display a foliated aspect characterized by alternative fine light (plagioclase-rich) and large dark (amphibole-rich) bands. Mylonites are the most represented rock types in both the FKSZ and NMSZ where they occur

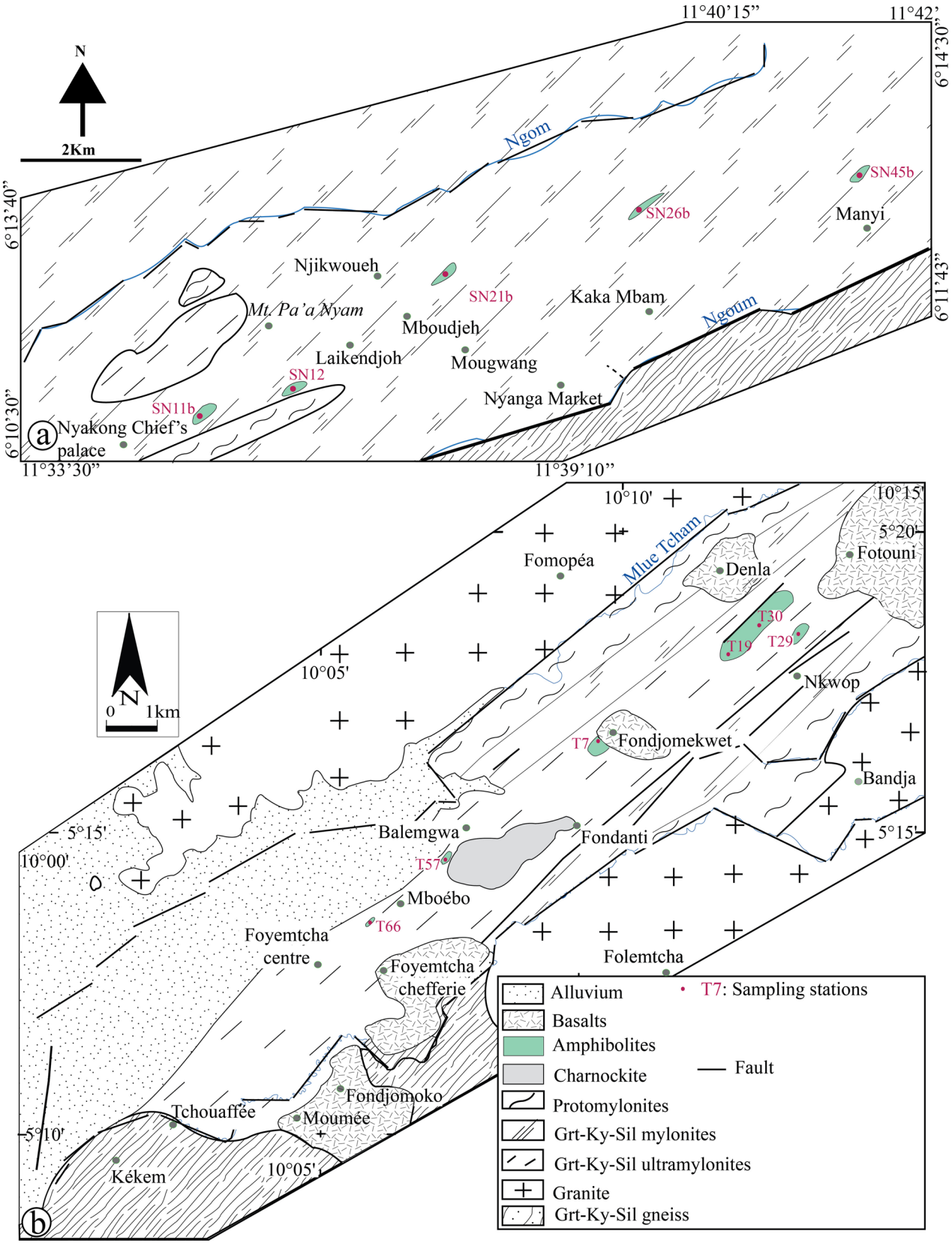

Fig. 3 Geological map of the study areas showing the sampling stations in the NMSZ (**a**) and FKSZ (**b**)

Table 1 Major, trace and rare Earth elements analyses

Rock types	Pyroxene amphibolite								
Sample numbers	T7	T19	T57B	T66C	SN11B	SN12B	SN45B	SN26B	SN21B
Major elements (wt %)									
SiO2	58.16	58.91	50.90	45.66	53.56	50.58	46.74	48.49	50.34
Al2O3	15.52	15.22	15.60	12.27	16.58	15.73	11.66	12.00	16.34
Fe2O3	6.56	6.56	9.30	13.55	8.86	12.18	11.36	10.69	10.01
CaO	5.56	5.26	9.54	12.27	6.45	9.40	10.70	10.09	8.55
MgO	5.26	5.00	7.54	9.08	4.11	5.15	13.73	10.39	7.56
Na2O	3.48	3.53	2.90	0.98	3.23	0.81	0.79	2.17	2.79
K2O	3.06	3.95	0.92	0.94	2.65	1.72	1.16	2.65	1.44
TiO2	0.84	0.82	0.97	3.29	2.11	2.08	0.91	1.28	1.18
MnO	0.10	0.10	0.14	0.20	0.11	0.20	0.18	0.17	0.14
P2O5	0.35	0.36	0.20	0.51	0.94	0.28	0.18	0.52	0.34
Total	98.89	99.71	98.02	98.75	98.60	98.11	97.42	98.45	98.70
Traces elements (ppm)									
Ba	476.29	1891.15	556.32	221.56	1505	459	271	1285	879
Cr	232	263	217	412	120	80	910	540	400
Cs	1.61	2.12	0.25	0.30	2.18	0.35	0.18	0.96	0.39
Ga	21	21	16	21	23.2	21.3	14.3	18.2	17.8
Hf	0.87	1.20	0.92	3.17	6.4	6.3	1.7	4.8	3.3
Nb	10.86	15.85	8.15	62.48	25.6	29.1	2.9	11.9	10
Rb	71.74	119.02	30.59	27.54	126.5	80.6	39.1	97.6	39.5
Sn	1.18	1.71	0.92	3.55	2	4	5	2	1
Sr	1571.43	1030.61	732.51	557.12	1025	381	165	611	739
Ta	0.52	0.86	0.35	2.52	1.4	1.9	0.2	0.5	0.6
Tb	0.70	0.76	0.61	1.16	0.93	1.2	0.66	0.96	0.69
Th	7.12	5.99	1.46	3.93	13.05	3.89	0.87	1.76	1.51
U	0.73	1.19	0.23	1.33	1.63	0.94	0.47	0.35	0.31
V	117	118	168	323	157	291	174	232	179
W	0.21	0.42	0.25	1.01	1	1	1	1	1
Y	17.92	21.24	16.24	30.30	19.3	34.3	15.9	22.8	17.2
Yb	1.44	1.78	1.30	2.23	1.47	3.61	1.44	1.8	1.54
Zr	26.41	41.28	27.24	107.95	258	242	55	188	124
Cu	17.03	14.87	26.35	13.74	–	–	–	–	–
Co	25.76	24.80	40.21	55.65	–	–	–	–	–
Li	32.15	22.30	10.10	6.77	–	–	–	–	–
Ni	89.85	82.43	183.78	181.12	–	–	–	–	–
Pb	36.49	32.10	4.62	8.02	–	–	–	–	–
Sc	18.43	18.72	35.96	41.61	–	–	–	–	–
Zn	82.93	72.63	100.03	124.40	–	–	–	–	–
Rare earth elements (ppm)									
La	83.20	71.44	27.66	45.69	81.1	28.8	15.1	38.8	21.3
Ce	134.12	125.28	57.93	92.87	169	66.3	36.8	89.4	46.9
Pr	16.69	15.07	7.71	12.12	19.3	8.32	5.13	11.4	5.88
Nd	60.26	54.12	31.16	48.62	25.6	29.1	2.9	11.9	10
Sm	9.46	8.66	5.79	9.50	12.35	7.99	5.15	9.86	5.48
Eu	2.74	2.08	1.91	2.99	2.67	2.18	1.72	2.23	1.61
Gd	6.64	6.55	4.82	8.69	7.38	7.68	4.22	7.05	4.49
Tb	0.70	0.76	0.61	1.16	0.93	1.2	0.66	0.96	0.69
Dy	3.67	4.14	3.44	6.58	4.22	6.63	3.26	4.6	3.54

Table 1 (continued)

Rock types	Pyroxene amphibolite								
Sample numbers	T7	T19	T57B	T66C	SN11B	SN12B	SN45B	SN26B	SN21B
Ho	0.64	0.73	0.60	1.14	0.74	1.31	0.64	0.89	0.7
Er	1.76	2.02	1.60	2.94	1.91	3.71	1.62	2.33	1.78
Tm	0.22	0.27	0.20	0.35	0.25	0.52	0.26	0.31	0.27
Yb	1.44	1.78	1.30	2.23	1.47	3.61	1.44	1.8	1.54
Lu	0.20	0.25	0.17	0.29	0.22	0.49	0.19	0.31	0.22
∑REE	795.40	717.60	383.70	639.20	327.14	167.84	79.09	181.84	104.4
Eu/Eu*	1.10	0.80	1.10	1.10	0.86	0.85	1.78	0.83	0.55
Ce/Ce*	0.88	0.94	0.97	0.97	1.05	1.05	1.03	1.04	1.03
$(Ba/La)_N$	1.36	6.27	4.77	1.15	4.40	3.78	4.25	7.85	9.78
Gd/Yb	3.80	3.05	3.07	3.22	4.15	1.76	2.42	3.24	2.41
$(La/Sm)_N$	5.68	5.33	3.08	3.11	4.24	2.33	1.89	2.54	2.51
$(Sm/Yb)_N$	7.28	5.41	4.95	4.73	9.33	2.46	3.97	6.09	3.95
$(Th/Yb)_N$	0.84	0.57	0.19	0.30	1.51	0.18	0.10	0.17	0.17

as slab stones in riverbeds, on hillsides and road trenches. Depending on the deformation intensity, three types of mylonites are distinguished: protomylonites (less deformed), *stricto senso* (ss) mylonites (moderately deformed), and ultramylonites (strongly deformed). Protomylonites are located on the borders of the Fomopéa and Bandja plutons in the FKSZ and as rock pocket in ultramylonites in the NMSZ. They are rich in sheared and fractured porphyroclasts of hornblende, plagioclase, K-feldspar, and pyroxene within a matrix composed of biotite and quartz. Mylonites and ultramylonites crop out toward the core of the FKSZ while ss mylonites occur on the borders of the NMSZ. They consist of eye-like clasts or lenses-like garnet crystals, K-feldspar clasts, and ribbon quartz aligned and oriented NE-SW. Microscopic observations indicate that these rocks are composed of porphyroclasts, porphyroblasts, clasts, and blasts of garnet, kyanite, K-feldspar, and plagioclase in a very fine crushed matrix made up of quartz and biotite. Charnockites outcrops as slab stones or boulders on hilltops or hillslopes, in valleys, and riverbeds within ultramylonites or as veins in garnet-kyanite-sillimanite gneiss in the FKSZ. It consists of quartz, feldspar, plagioclase, orthopyroxene, and biotite. Based on mineral parageneses from kyanite-sillimanite-garnet gneisses as well as microstructures, Sobze Yemdji et al. (2023) and Tcheumenak Kouémo et al. (2023) drew conclusions that this rock type underwent high-grade regional polyphasic metamorphism in the granulite facies and later on, was overprinted by high-pressure mylonitization during the early sinistral and late dextral shear deformations phases.

From the above it is worth noting that mylonites and gneiss have been studied in detail and used for correlation compared to amphibolites (Sobze Yemdji et al. 2023; Tcheumenak Kouémo et al. 2023). By contrast, the tectonic and metamorphic history, as well as the geodynamic significance of amphibolites are not known. Are these amphibolites pre- or post- D_1? The limited outcrops of amphibolites in these two shear zones (FKSZ and the NMSZ) only lead to an overview on those rocks and by combining them; they give better understandable lithotectonic and geodynamic information.

Methods

Samples collection for microstructural analyses and thermobarometric studies

From each rock-type, oriented fresh samples were collected during field works. Samples for thin sections were prepared in the Institute for Geological and Mining Research laboratory where each of them was cut parallel to the XZ plane. Thin sections were partly (samples T7, T19, T57B and T66C) obtained at the Geowissenschaftliches Zentrum der Georg-August-Universät Göttingen, GZG, of the University of Göttingen, Germany. Eleven (11) thin sections of pyroxene amphibolite were obtained. They were described under polarized microscope at the Laboratory of Environmental Geology of the University of Dschang, Cameroon. Microstructures and metamorphism critical minerals such as pyroxene and amphibole were used as indirect method for metamorphism *P–T-t* path reconstruction. Indeed, the rock fabric and the mineral geometry and assemblages reflect the deformation mechanism and the grade recorded and partially or totally preserved by the rock in a particular metamorphic grade/facies. This thus, enables the metamorphism *P–T-t* path estimation and reconstruction (Pons 2001; Ten Grotenhuis et al. 2003; Passchier and Coelho 2006; Bouyo Houketchang et al. 2013; Tcheumenak Kouémo et al. 2023). Some

microstructures and diagnostic mineral assemblages, help in characterizing features of particular metamorphic facies. For example the occurrence of, (i) amphibole fishes are characteristic microstructures that can be used for amphibolite facies, (ii) regular and straight mineral boundaries, (iii) triple points formed by some minerals like plagioclase, pyroxene and amphibole characterize the high-grade amphibolite to low grade granulite metamorphic facies (Ten Grotenhuis et al. 2003; Passchier and Coelho 2006; Bouyo Houkentchang et al. 2013; Owona et al. 2013; Tcheumenak Kouémo et al. 2023).

Analytical techniques

Whole—rock geochemical analyses

For the present study, nine representative amphibolites samples of the ten collected, were prepared and analyzed for whole-rock geochemistry (Table 1). Whole rock analyses for Major and trace elements were performed by X-ray fluorescence and ICP–MS at the Geowissenschaftliches Zentrum Göttingen, Georg-August Universität, Abteilung Geochemie, Germany (for samples T7, T19, T57B and T66C) and the Mineral Laboratory of the Bureau Veritas Minerals, Canada (for samples SN11B, SN12B, SN45B, SN21B and SN26B). The determination of major elements and some trace elements (Sc, V, Cr, Co, Ni, Zn, Ga, Rb, Sr, Zr and Ba) was performed using X-ray fluorescence analysis on glass discs. The preparation of glass discs was done by mixing sample powders with lithium metaborate prefused lithium tetraborate and LiF in platinum-gold crucibles and fused at 1150 °C for 20 min. About 60 reference materials were used for major and trace elements calibration. These references are from a wide variety of international geochemical reference samples including the National Institute of Standards and Technology, the South African Bureau of Standards, the Geological Survey of Japan, the National Research Council of Canada, the US Geological Survey, the International Working Group 'Analytical standards of minerals, ores and rocks'. The major elements' analytical uncertainty (2σ) was less than 1% (except for LOI: c. 10% and Na: 2%). The trace elements' analytical precision (2σ) was 5%. ICP–MS analysis was performed for other additional trace elements. The analytical errors for Nb and Ta were about 15–20% and 10% for other trace elements according to estimation from rock standards JB3 and JA2.

Rb–Sr and Sm–Nd isotopic analyses

About 100 mg of the whole-rock samples digested by a mixture of HNO_3 and HF acid at a temperature of 180 °C were used to perform the first step. Sr and rare earth elements (REE) separation were performed using cation exchange resin AG 50W-X8 with 2.5 M HCl filled columns. Hexyl di-ethyl hydrogen phosphate-coated Teflon with 0.18 M HCl filled columns were used to separate REE from Nd. Measurements of Sr, Nd, Rb and Sm isotopes were performed using a Finnigan Triton mass spectrometer at the Geowissenschaftliches Zentrum Göttingen, Georg-August Universität, Abteilung Geochemie. Sr and Nd measurements were respectively performed in static and peak-jumping multicollector mode. Sr and Nd analyses corrections were done for mass fractionation by normalization to 88Sr/86Sr = 8.375209 and to 146Nd/144Nd = 0.7219 respectively. The average value of 0.710244 was obtained from repeated measurements of the standard NBS987, with reproducibility of 0.000007 (2σ). The Nd standard La Jolla was determined with an average of 0.511845 + 0.000005. The blanks were negligible for Sr ranging from 100 to 200 pg and for Nd c. 100 pg.

Results

Petrographic, structural and microstructural data

Petrography

Pyroxene amphibolite (PA) occurs as slab stones which sometimes restite-like in migmatites (Fig. 4a, b), banded to lenses-like (Fig. 5c–e), egg-like enclaves (Fig. 5g, h), folded bands (Fig. 5d), sheared (Fig. 5b, e, f) and/or boudinaged (Fig. 5e, h) green to dark green displaying NE-SW preferred orientation in FKSZ and NMSZ (Fig. 5c–h) in paragneiss. PA displays heterogranular nematoblastic texture (Fig. 4c–i) marked by amphibole, plagioclase and clinopyroxene porphyroblasts dispersed in between medium grained crystals of amphibole, plagioclase and clinopyroxene (Fig. 5a–f) displaying preferred orientation (Figs. 4c, d, f, 5f) mainly consisting of amphibole and plagioclase. In addition, some mylonitized amphibolites display Hornblende pophyroclasts grained boundaries granulation in a dynamically recrystallized quartz + feldspar matrix in FKSZ (Fig. 4d, e) and NMSZ (Fig. 5f). Amphibole (60%) is subeuhedral to anhedral, displays regular to lobate grained boundaries occupied by plagioclase, quartz and opaque minerals (Fig. 4b, c), with some crystals showing quartz inclusions (Fig. 4d, e). Plagioclase (≈ 20%) is anhedral and occurs as crystal aggregates and display grained boundaries dynamic recrystallization marked by sharp crystals limits defining triple points (Fig. 4g), mechanical and curved twinning symptomatic of high-grade deformation (Fig. 4c) or associated to opaque mineral around amphibole (Fig. 4e). Clinopyroxene (15–20%) is anhedral and occurs as stable or retrograde crystals (Fig. 4c, h, i). Parageneses involving

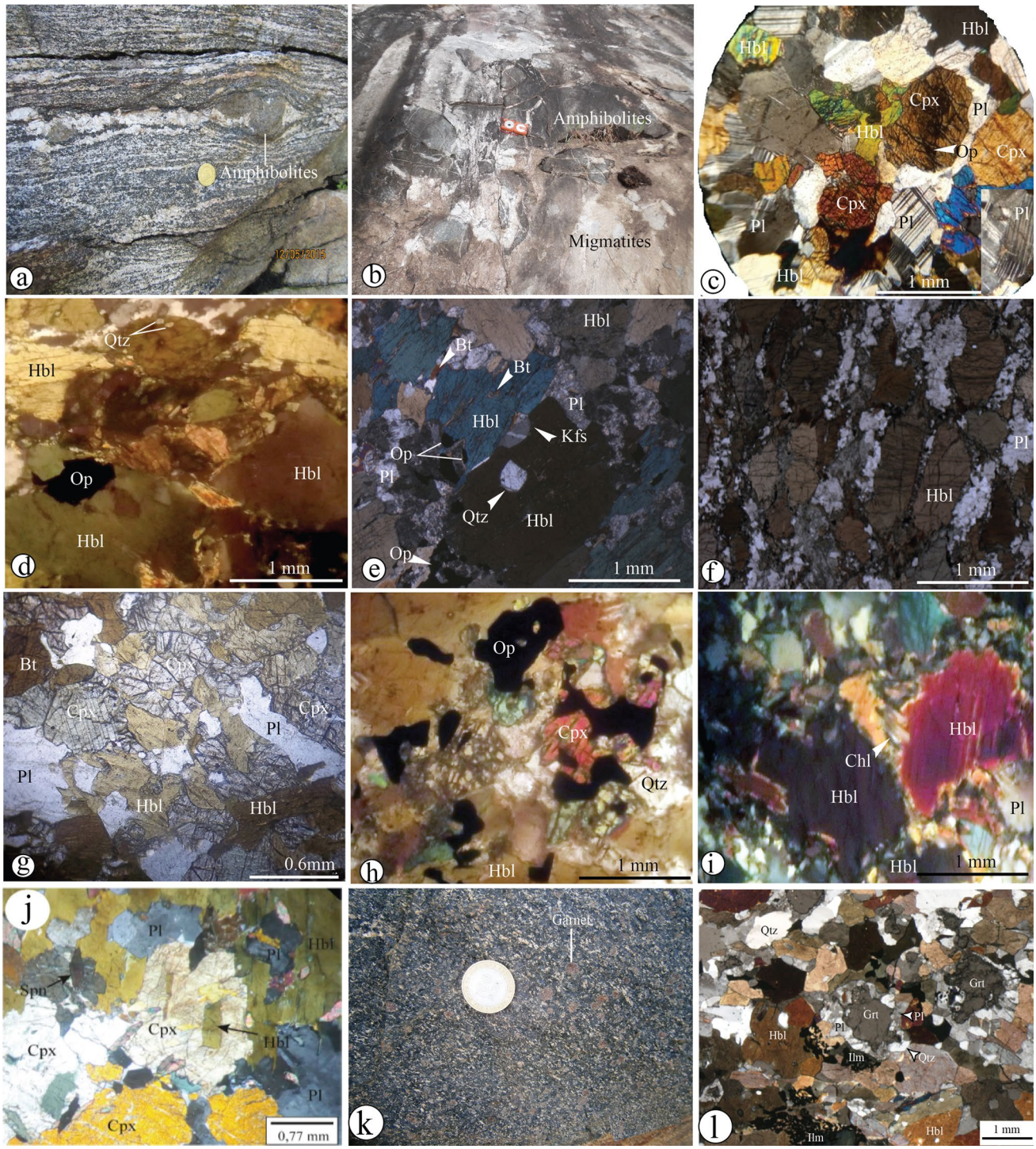

Fig. 4 Photographs and Microphotographs of pyroxene and garnet amphibolites. **a** Boudinaged lenses of amphibolites in paragneiss in Nyakong. **b** restite-like amphibolites in migmatite in Nyakong. **c–e** Heterogranular nematoblastic texture of pyroxene amphibolite showing clinopyroxene crystals displaying regular boundaries. Note also the presence of fish-like amphibole (**d**). **f** lens-like amphibole showing preferred crystal orientation and plagioclase rims around the crystal. **g** Sharp grained boundaries displayed by plagioclase. **h** Retrograde transformation relic-like clinopyroxene crystals into hornblende and opaque minerals. **i** Anhedral amphibole displaying lobed contours and retromorphic transformation into chlorite. **j** Clinopyroxene crystals displaying hornblende inclusion. **k**, **l** Garnet amphibolite showing retromorphic garnet crystals displaying coronitic microstructures

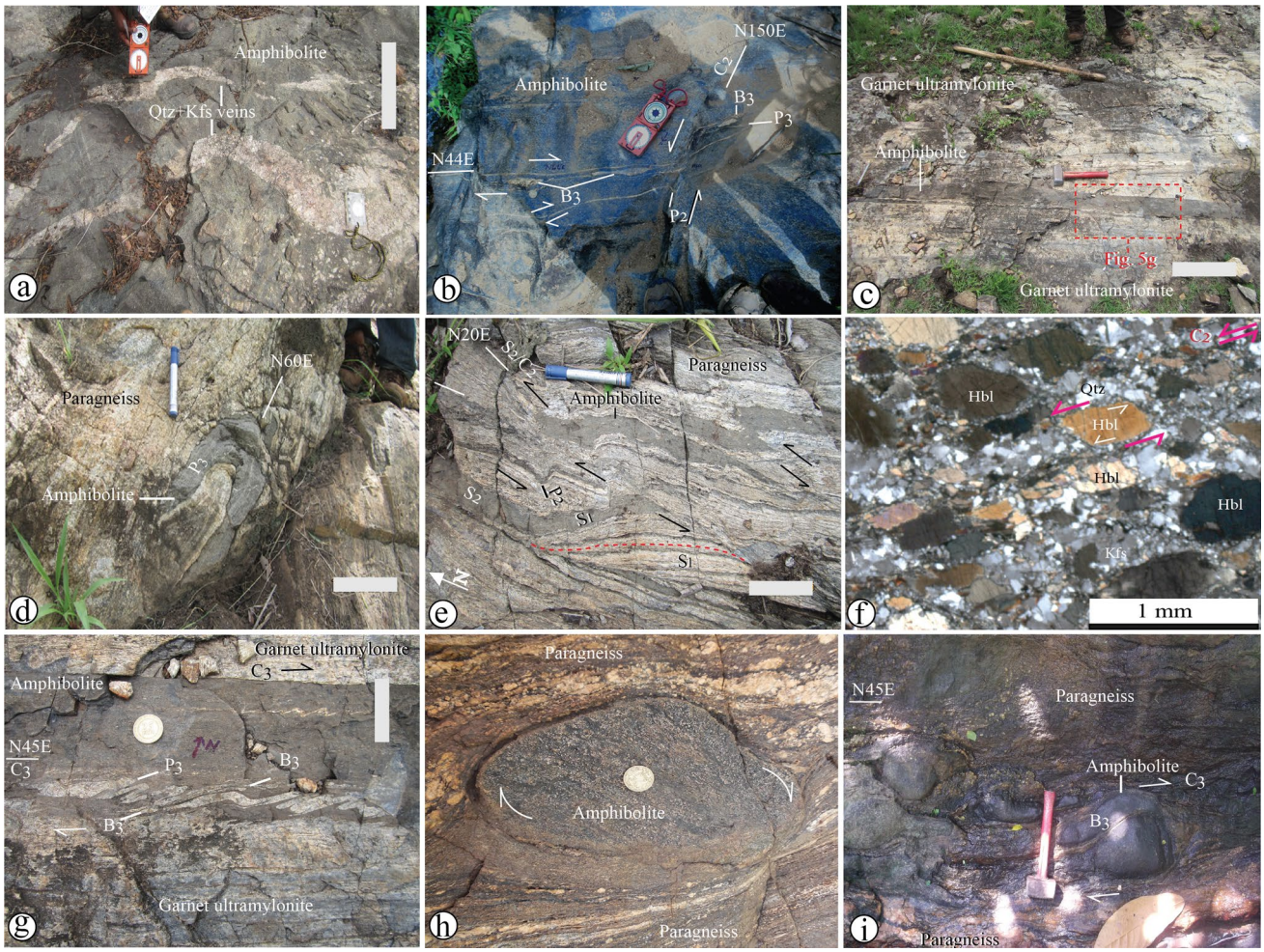

Fig. 5 Field structures and microstructures of the study areas. **a** Slab stone of PA outcropping as restite in NMSZ (a) and FKSZ (**b**). **c**, **d** Sheared (**c**) and folded in to P_3 fold (**d**) of PA veins respectively in garnet ultramylonite and orthogneiss. **e** D_2 deformation phase related field structures marked by NNE-SSW C_2/S_2 shear plane/foliation and P_2 folds transposing the S_1 foliation. **f** Preferred orientation of lens-like amphibole crystals showing sinistral syn-D_2 deformation. **g–i** D_3 deformation phase related field and microstructures marked by NE-SW C_3/S_3 shear plane/foliation and P_3 fold transposing the S_2 foliation (**g**), sigmoid (**h**) and B_3 boudins (**i**)

stable clinopyroxene consist of hornblende + clinopyroxene + plagioclase association (Fig. 4c). Retrograde clinopyroxene occurs as relic-like crystals with hornblende and opaque minerals replacing this mineral' primary phase. Paragenesis involving the retrograde phase consists of hornblende + clinopyroxene + plagioclase ± quartz + opaque minerals association (Fig. 4e–h). Biotite (≈ 5%) is sheet-like aggregates (Fig. 4e) and interstitial crystals in between hornblende porphyroblasts (Fig. 5a, c). It also occurs as shapeless crystals in amphibole cleavages (Fig. 4e). Quartz (≤ 5%) occurs as very fined grained or stretch ribbon crystals associated to amphibole or as inclusion in this mineral (Fig. 4b, c). Opaque minerals (< 5%) occur as shapeless crystals around or in amphibole and clinopyroxene cleavages (Fig. 4c–e, h). Since the opaque mineral is intruding within the clinopyroxene crystals for example suggests a replacement relation; thus symptomatic of retrograde transformation of these minerals (Fig. 4h). Some large grained crystals occur as substitution totally replacing preexisting clinopyroxene in amphibolite from FKSZ (Fig. 4d). Chlorite is observed to be replacing amphibole from its boundary (Fig. 4i). In Bankim, located between NMSZ and FKSZ (Fig. 1b), pyroxene and garnet are present in amphibolites (Fig. 4j–g), with some pyroxene crystals displaying amphibole inclusion (Fig. 4j). Garnet (≈ 10%) is mostly lense-like to round (few crystals) shaped displaying lobate contours. It shows coronitic textures characterized by lobate contours' garnet crystals rimed by hornblende, plagioclase, quartz and ilmenite (Fig. 4l). This mineral paragenesis defines a kelyphitic microstructure characterized by garnet + hornblende + plagioclase + ilmenite parageneses (Fig. 4l).

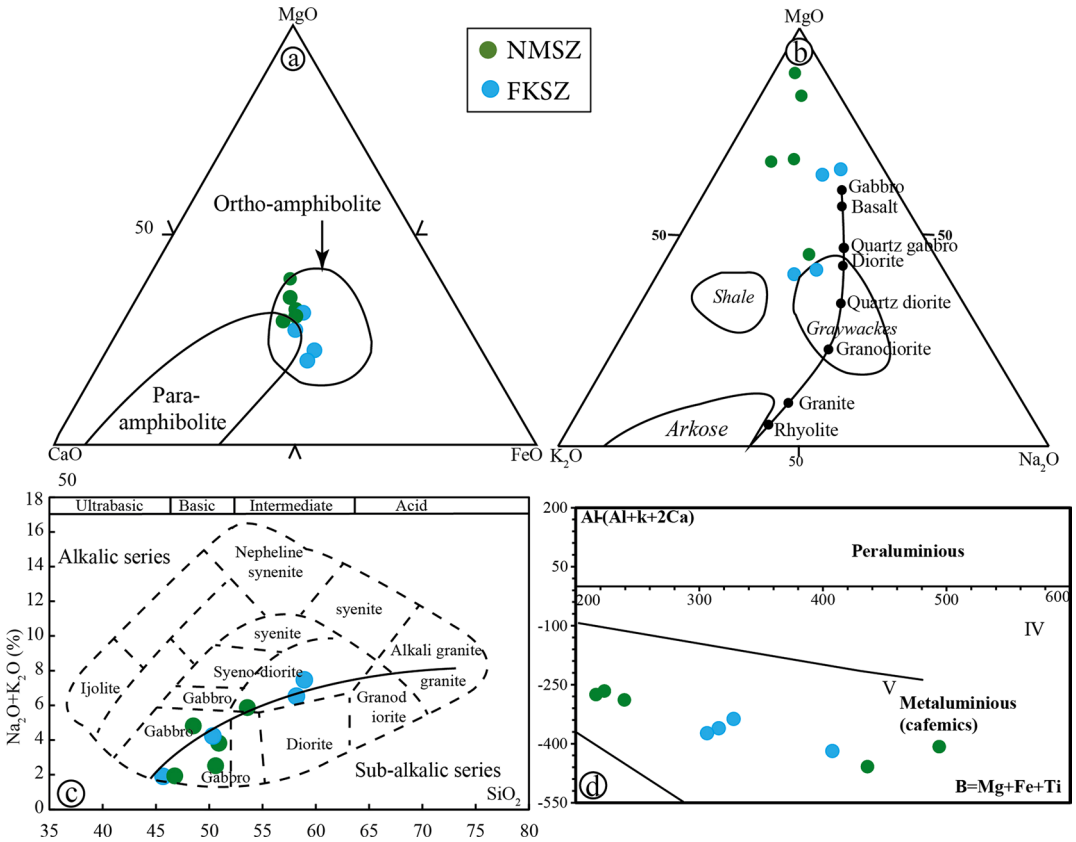

Fig. 6 Geochemical characteristics of amphibolites from FKSZ and the NMSZ areas in the MgO-CaO-FeO (Walker et al. 1959), MgO-K_2O-Na_2O (De La Roche 1965), Na_2O+K_2O vs SiO_2 (Le Maître et al. 1989) and (Al + K + 2Ca) vs (Fe + Mg + Ti) (Debon et Le Fort, 1983) diagrams showing the igneous (**a**, **b**) gabbroic (**c**) origine of their protolites and metaluminious character (**d**). IV and V = metaluminious rocks, IV = biotite + amphibole ± pyroxene, V = clinopyroxene ± amphibole ± biotite domains

Structures and microstructures

Structural features displayed by amphibolites from FKSZ and NMSZ indicate three deformation phases (D_1, D_2 and D_3) as shown by slab stones (Fig. 5a, b), bands (Fig. 5c–f), lenses, enclaves and sigmoids (Fig. 5g–i) of these rocks. Slab stones occur as restites, cut across by quartz-K-feldspar-rich veins in migmatites in Nyakong (Figs. 4b, 5a). Lenses are folded, boudinaged or transposed in paragneiss and ultramylonites (Figs. 4a, 5d–g). Sigmoid shapes are displayed by amphibole crystals which show sinistral movement (Fig. 5d–g) or by amphibolites enclaves (Fig. 5f) and boudins (Fig. 5h, i). The D_1 deformation phase is characterized by NW–SE (N135E-N155E) remnant foliation (S_1) gently (19°-29°) dipping towards NE (Fig. 5e). This NW–SE foliation almost entirely transposed by sinistral shear planes, occurs as relics (Fig. 5e). The D_2 phase is characterized by N-S to NNE-SSW (N20E-N27E) sinistral shear planes C_2 and associated S_2 foliation defining the C_2/S_2 as well as the associated P_2 knee-like shear folds gently dipping (20°-30°) towards the south (Fig. 5c–h). The sinistral shear markers also include B_2 shear band boudins form as results of rhythmic transposition of amphibolite lenses by series of N20E C_2 shear planes (Fig. 5e) and σ-type sigmoids display by asymmetric amphibole fishes (Fig. 4f). N150E C_2 shear planes are also recorded in amphibolites from FKSZ (Fig. 5b). The D_3 phase is a clockwise shear phase, characterized by dextral shear markers. These dextral shear markers include: (i) NE-SW C_3 planes (Fig. 5b, f, h, i), responsible for the development of (ii) S_3 foliation with strike parallel to C_3 planes; (iii) lens-like and fish-like structures (Fig. 4f, d, 5i,); (iv) B_3 shear band boudins (Fig. 5f, h) and (v) P_3 recumbent and overturn folds, respectively display by amphibolite lenses and quartz-K-feldspar rich light bands in amphibolites lenses (Fig. 5b, d, g). They show short and long limbs and display gentle plunges (10°-15°) axes towards the NE or SW (Fig. 5d, f); (v) σ-type sigmoids (Fig. 5b, e, i), (vi) asymmetric amphibole fishes (Figs. 4f, 5b); (vii) sharped and polished grained boundaries (Fig. 5a–d) and (viii) triple points (Fig. 5c, d) display by amphibole crystals. Also mylonites and ultramylonites display matrix with dynamically recrystallized quartz + K-feldspar and Hbl pophyroclasts grained boundaries granulation (Fig. 4f).

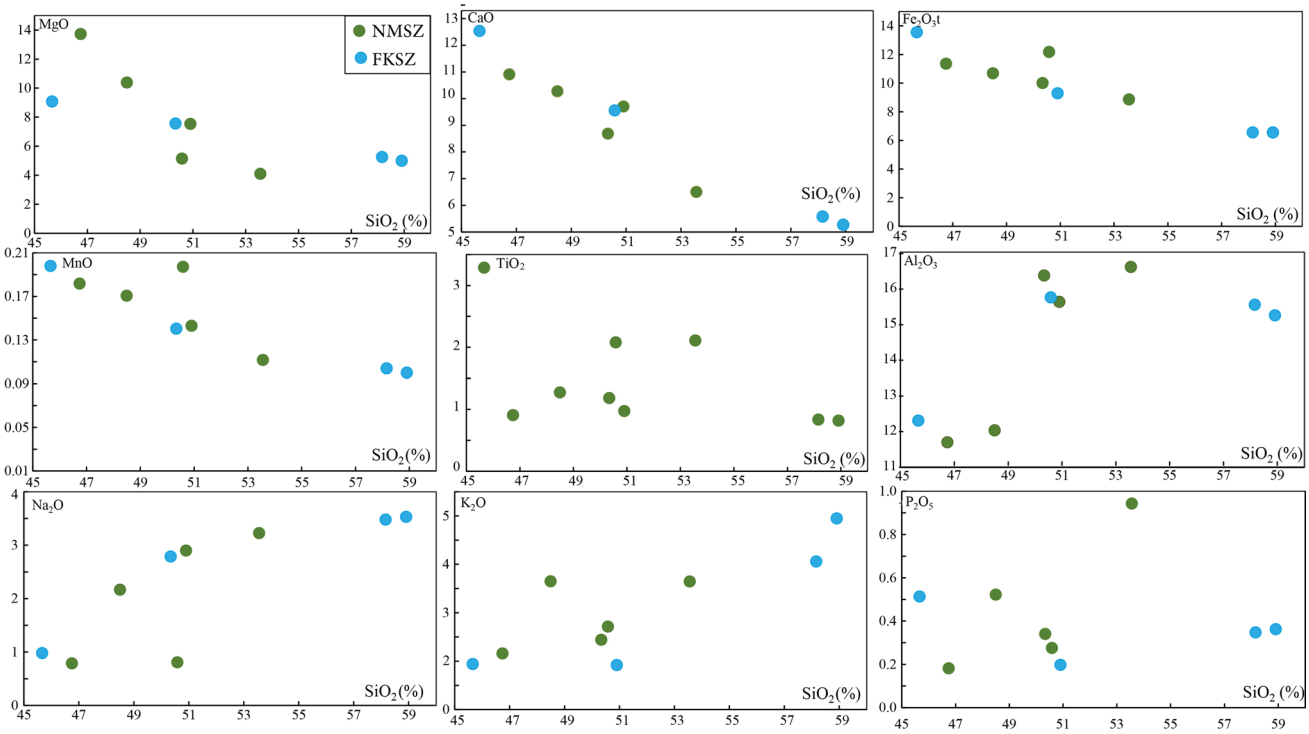

Fig. 7 Harker diagrams of selected major elements

Geochemistry

Classification

PA from the FKSZ and NMSZ entirely plot in the ortho-amphibolite and gabbros to diorite domains respectively in the CaO-MgO-FeO and K_2O-MgO-Na_2O of Walker et al. (1959), De La Roche (1965) and Le Maître et al. (1989) diagrams (Fig. 6a–c). They are mostly sub-alkaline (Fig. 6c).

Major elements

Representative samples of PA from FKSZ (n = 4) and NMSZ (n = 5) analyzed for major and trace elements are presented in Table 1. Major elements data analysis indicates that amphibolites from FKSZ and NMSZ display approximately the same variation intervals (Table 1). SiO_2 (45.66–58.91 wt%), Al_2O_3 (11.55–16.27) wt% and Fe_2O_3 (6.56 to 13.55 wt%) display variable contents as other major oxides (P_2O_5, CaO, MgO, Na_2O, K_2O, TiO_2) (Table 1). Negative correlation is displayed by binary plot of SiO_2 (wt%) versus CaO, Fe_2O_3, MgO and MnO (Fig. 7), while positive correlation is observed for Al_2O_3, K_2O and Na_2O (Fig. 7).

Trace elements

Trace element concentrations (ppm) display strong variations in amphibolites throughout both FKSZ and NMSZ (Fig. 8, Table 1). REE data displays higher concentration (ΣREE = 383.74–795.36 ppm) in amphibolites from FKSZ compared to those from NMSZ (ΣREE = 79.09–327.14 ppm) (Table 1). Spider diagram from normalized REE to chondrite indicates (Fig. 9a): (i) enrichment of REE compared to the chondrite values; (iii) slightly and prominent negative (Ce/Ce* = 0.88–0.97) and slightly positive (Ce/Ce* = 1.03–1.05) cerium anomalies respectively in the FKSZ and NMSZ; (iv) negative (Eu/Eu* = 0.55–0.86) to slightly positive (Eu/Eu* = 1.10–1.78) europium anomaly. The REE profiles are generally more fractionated in LREE $(La/Sm)_N = 1.89–5.68$ thanHREE $(Gd/Yb)_N = 1.76–4.62$.

The MORB-normalized (Pearce 1983) spider diagram patterns (Fig. 9b) displays (i) K, Rb, Ba (except for sample T7 and T66C which displays slight negative Ba anomaly), Th, Ce and Sm positive anomalies (Fig. 9b) and (ii) Ta-Nb (except for sample T66C which displays slight positive Nb anomaly) and Zr-Hf negative anomalies.

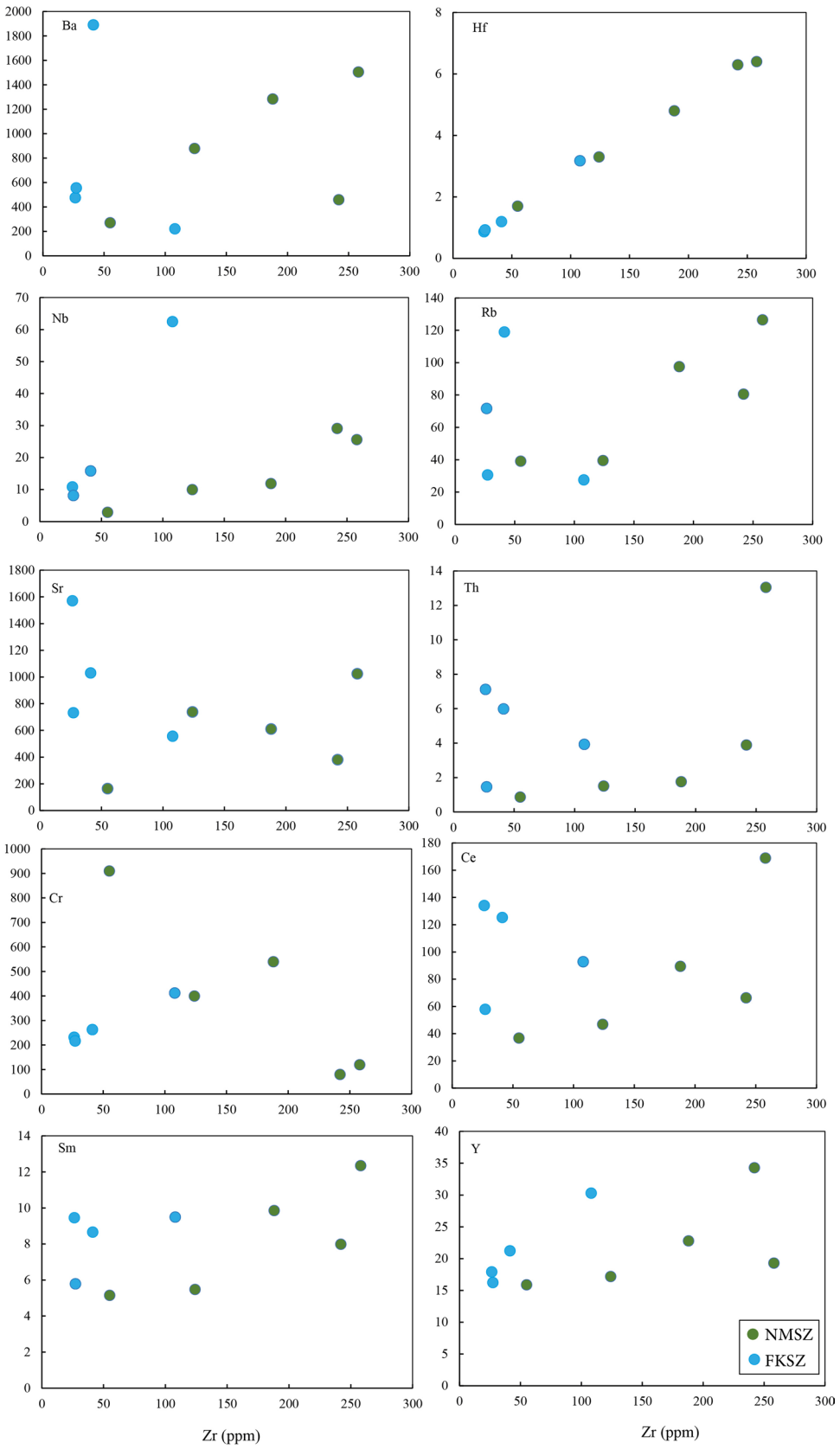

Fig. 8 Harker diagrams of selected trace elements

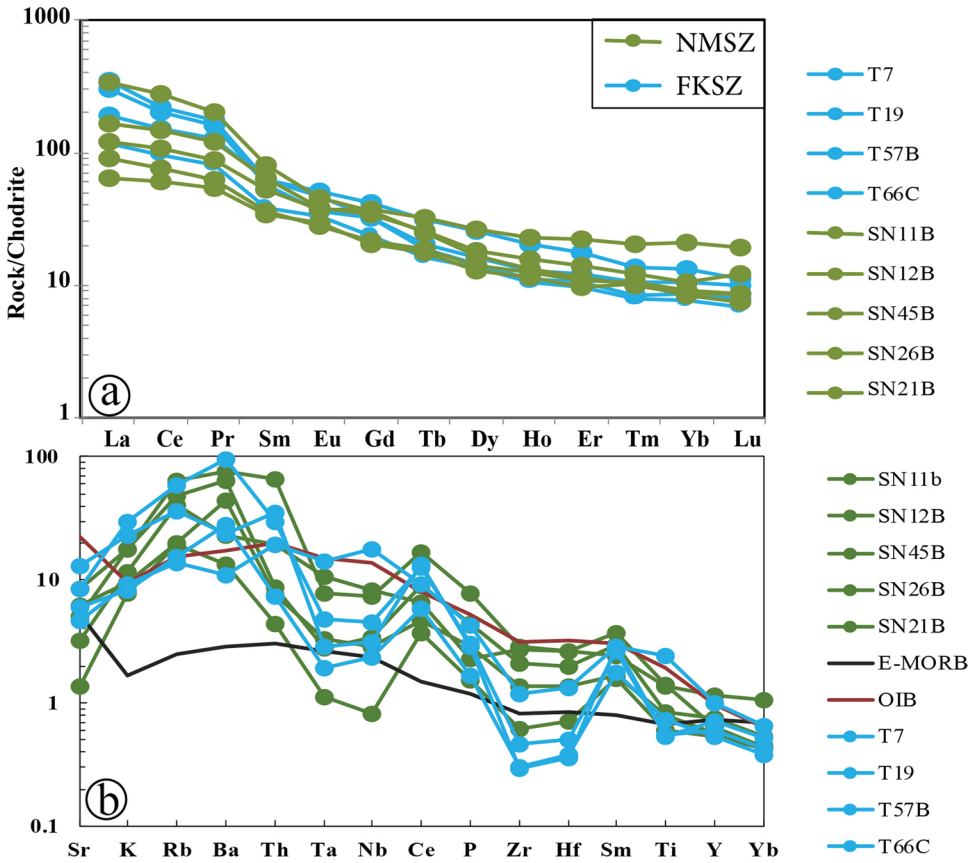

Fig. 9 Normalized spider diagram patterns for Bankim amphibolites. **a** Chondrite-normalized REE to Mc Donough and Sun (1995) values. **b** MORB-normalized to Pearce (1983) values arachnogram patterns

Rb–Sr and Sm–Nd isotopic compositions

Metamorphic U–Pb zircon age is constrained around 600 Ma for metabasites and metapelites along the CCSZ (Tchaptchet Tchato et al. 2009; Bouyo Houkentchang et al. 2009, 2013). Individual $^{87}Sr/^{86}Sr$ initial ratios calculated at 600 Ma (U–Pb zircon age) is 0.70488 (Table 2). Nd isotopes from sample T66C display positive ƐNd of + 1.27 with Nd T_{DM} age of 1248 Ma (calculation based on Goldstein 1988 model), that may indicate a mesoproterozoic crust (Table 2).

Discussion

Structural evolution

Deformation structures recorded by amphibolites from the FKSZ and NMSZ are classified from the oldest to the younger into D_1, D_2 and D_3 (Fig. 10). The D_1 phase, with σ_1 applied in the NE-SW direction (Fig. 10a), is poorly represented since it is the early deformation phase whose structures were almost wiped out or transposed by the late phases D_2- and D_3-related structures (Fig. 5e). It is represented by the S_1 foliation which displays NW–SE trend indicating that the main stress direction σ_1 was applied in the NE-SW direction (Figs. 5e, 10a), compatible with the convergence of the Sahara metacraton over the Congo Craton (Efon Awoum et al. 2020; Achu Megnemo et al. 2021; Sobzé Yemdji et al. 2023) responsible for high-grade metamorphism around 600 Ma (Tchaptchet Tchato et al. 2009; Bouyo Houkentchang et al. 2013; Tcheumenak Kouémo et al. 2023). According to Kwékam et al. (2010) and Ngako et al. (2008), D_1 phase along the CCSZ is dated at 622–610 Ma while for Tchaptchet Tchato et al. (2009) and Bouyo Houkentchang et al. (2009, 2013) D_1 is dated around 600 Ma. The occurrence of amphibolites as restites in migmatites (field evidences of metamorphic peak), enclaves or lenses in paragneiss may indicate that their emplacement are pre-D_1 phase. This S_1 foliation was transposed by N-S to NNE-SSW sinistral shear planes during the D_2 deformation phase (Figs. 5e, 10b). The D_2 phase, with σ_1 applied in the WNW-ESE direction (Fig. 10b), is a shear phase, which developed structures such as shear band boudins (Figs. 5e, g; 10b), knee-like folds (Figs. 5b, e; 10b) and lens-like and fish-like structures displayed by amphibolites (Figs. 5f, 10b). The D_2 sinistral deformation phase is dated at 610–590 Ma and related to an early mylonitic event (Ngako et al. 2008, 2003; Tchaptchet Tchato et al. 2009; Njanko et al. 2010; Kwékam et al. 2010; Tcheumenak Kouémo et al. 2014, 2023). It is compatible

Table 2 Sr and Nd isotopic data

Rb	Sr	$^{87}Rb/^{86}Sr$	2σ	$^{87}Sr/^{86}Sr$	2σ	Sr_i600	Sm	Nd	$^{147}Sm/^{144}Nd$	2σ	$^{143}Nd/^{144}Nd$	2σ	εNd_0	εNd_{600}	$^{143}Nd/^{144}Nd_{600}$	T_{DM} (Ma)
25	542	0.13553	0.0054	0.706	0.000006	0.7049	8.81	44.33	0.12022	0.0024	0.5124	0.000002	− 4.6	1.27	0.5119	1248

with the convergence of the Sahara metacraton and West Africa Craton over Congo Craton around 600 Ma, which strongly affected the northern and western border of Cameroon (Tcheumenak Kouémo et al. 2023; Sobzé Yemdji et al. 2023). This phase is also responsible for the development of pull-apart basins and the emplacement of synkinematic pluton mostly along shear zones (Nguiessi Tchamkam et al. 1997; Tagne-Kamga et al. 1999; Kwékam et al. 2010, 2015, 2020a, b; Tcheumenak Kouémo et al. 2014, 2023; Efon Awoum et al. 2020; Achu Megnemo et al. 2021; Kamgang Tchuifong et al. 2022). D_3 is a NE-SW (N40E-N60E) dextral shear phase which is dated at 590–545 Ma and related to a late mylonitic event (Ngako et al. 2008, 2003; Tchaptchet Tchato et al. 2009; Njanko et al. 2010, Kwékam et al. 2010; Tcheumenak Kouémo et al. 2014, 2023, Sobzé Yemdji et al. 2023). The D_3 phase' evolution, with σ_1 applied in the NW–SE direction (Fig. 10c), led to the development of S_3 foliation (Fig. 10c), P_3 recumbent and overturn folds with gentle plunges towards the NE or SW (Fig. 5d, f; 10c1-c2), B_3 shear band boudins (Fig. 5f, h; 10c2, c4), σ-type sigmoids (Fig. 5b, e, i; 10c3-c4) and asymmetric amphibole fishes (Fig. 5h; 10c4).

Nature and origin of amphibolites

The amphibolites display high $(Fe_2O_3)_t$, CaO and MgO contents (Table 1), plot to the metabasalt domain in the Walker et al. (1959) and De La Roche (1965) diagrams (Fig. 6a, b) and metaluminous affinity (Fig. 6d) suggesting that they derive from a mafic protoliths. Their dominant basic character and the low SiO_2 content (45.66–58.91%) compatible with mantle-derived protoliths for these amphibolites, certainly suggests that they originated from the solid-state transformation of metabasite materials as indicated by Fig. 6c. This metabasites protolith originated from the melting of garnet lherzolite as indicated by Fig. 11a–c. This is evidenced by dominant oceanic crust character represented by the VAB and MORB nature displayed by PA from the FKSZ and NMSZ (Fig. 11d–f). The gabbroic protoliths to form oceanic crust, may have originated from garnet-lherzolite mantle as indicated by La/Sm and Sm/Yb ratios which are above the garnet-lherzolite melting curves (Fig. 11a–c) thus indicating that they are mantle reservoir derived products. This reservoir was slightly deeper than the garnet-spinel lherzolite level above 80 km depth, since the spinel-lherzolite and garnet-lherzolite transition zone corresponds to depths of about 70–80 km (Frey et al. 1991; McKenzie et O'Nions 1991; Kwékam et al. 2013).

The slightly positive εNd_{600Ma} (+ 1.27) (Table 2) indicated by T66C sample, suggests a mantle derived protoliths that underwent contamination by the continental crust. The Th/Yb vs Ba/La diagram (Fig. 11f) indeed indicate both

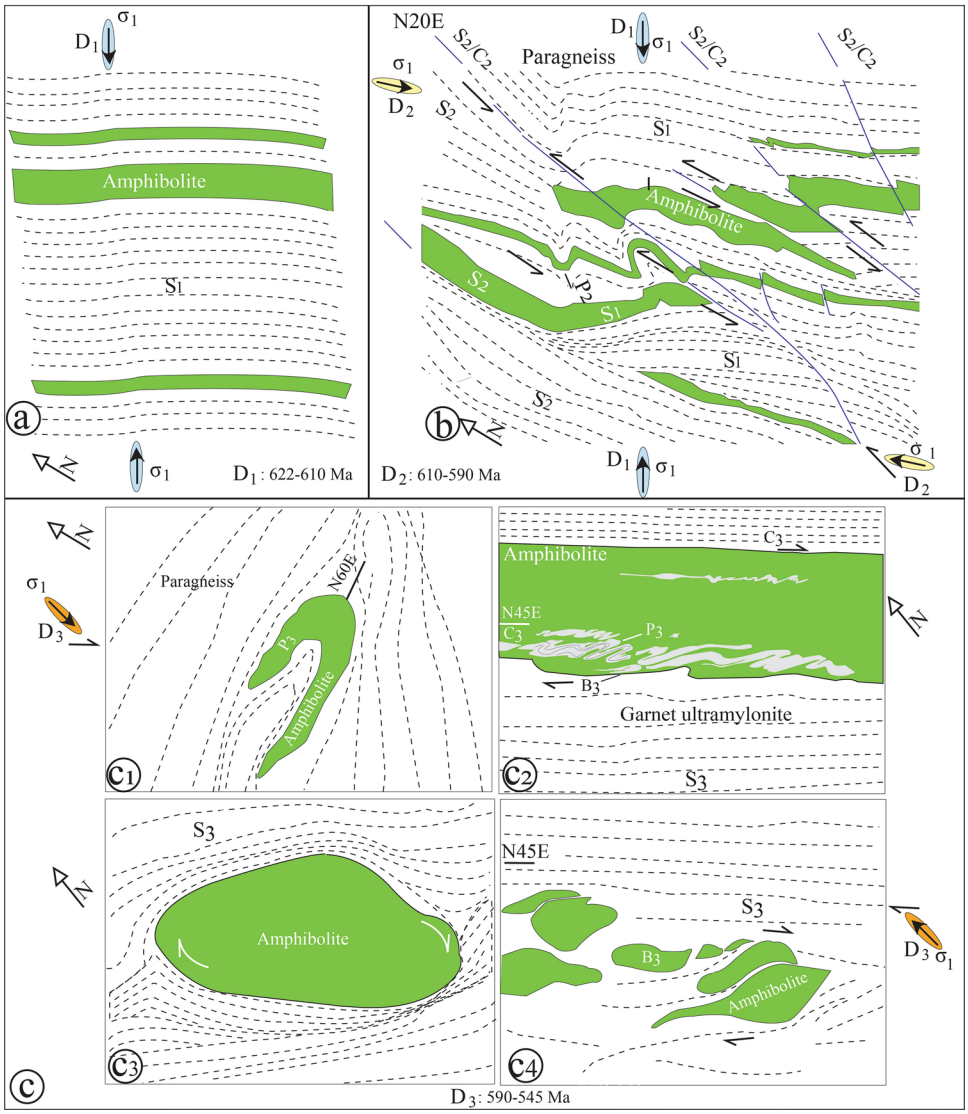

Fig. 10 Kinematic evolution model. **a** D_1 deformation phase and NW–SE S_1 foliation. **b** D_2 deformation phase and NNE-SSW C_2/S_2 shear plane/foliation and P_2 fold transposing the S_1 foliation. **c** D_3 deformation phase showing NE-SW C_3/S_3 shear plane/foliation and P_3 fold transposing the S_2 foliation, sigmoid and B_3 boudins. Note the application direction of the main stress σ_1, σ_2 and σ_3

subducted sediment and slab-derived fluids contributions for contamination that caused the metasomatism during the petrogenic process. The contribution of fluids (metasomatism) during the petrogenic process is evidenced by hornblende replacing clinopyroxene (Fig. 4b, e). In addition, during metamorphic processes especially when there is hydrothermal fluid participation in an orogenic belt like the CAFB, chemical element migration is common, certainly facilitated by fluids circulation. This is probably what underwent the protolith of these amphibolites.

The model age ($T_{DM} = 1.25$ Ga) with initial $^{87}Sr/^{86}Sr$ ratios of 0.70488 suggest an ancient Mesoproterozoic crustal (oceanic) source, formed from the melting of mantle at 1.25 Ga before it was recycled during the early stage of the Pan-African orogeny. Indeed, the studied area is located in an area that experienced multistage compressions from the Saharan metacraton to the north that tended to squeeze and the West African Craton to the west that tended to shear (Fig. 1a, b). This probably facilitate the emplacement of amphibolite lenses during the pre-Pan-African stage, thus pre-D_1. This ancient crust underwent metamorphic transformation during the collisional (burial) and post collisional (exhumation) stages of the Pan-African orogeny (Bouyo Houkentchang et al. 2013; Tcheumenak Kouémo et al. 2023). The FKSZ and the NMSZ are respectively located to the SW and the NE of the N30E-N50E branch of the CCSZ (Fig. 2), which displays a complex tectonic evolution, including a high-grade metamorphism. The resulting high-grade metamorphism' petrographic evidences are migmatites, gneisses (para- and ortho- gneisses) and metabasites (amphibolites) (Bouyo Houkentchang et al. 2013;

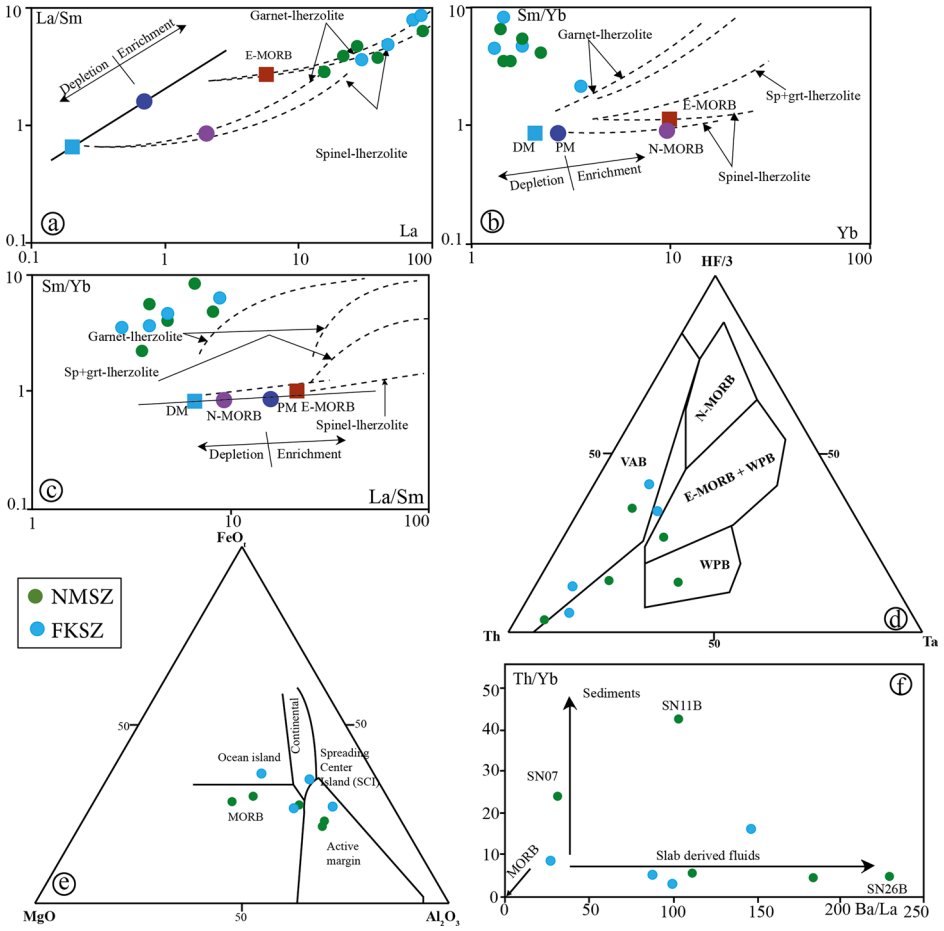

Fig. 11 REE and oxide discrimination diagrams. REE variations of La vs La/Sm (**a**), Sm/Yb vs Sm (**b**) and Sm/Yb vs La/Sm (**c**) after (Green 2006) showing the samples of FKSZ and NMSZ amphibolites. **d** Hf/3-Th-Ta discrimination diagram after Wood (1980). **e** Diagramme MgO-FeO_t-Al_2O_3 after Pearce et al. (1977). **f** Ba/La vs Th/Yb, diagrams after (Green 2006). WPA within-plate alkalic basalt; WPT, within-plate tholeiitic basalt; P MORB, plume mid-ocean ridge basalt; N MORB, normal mid-ocean ridge basalt; VAB, volcanic arc basalt; WPB, within-plate basalt; E-MORB, enriched mid-ocean ridge basalt. The compositions for Mantle array defined by depleted MORB mantle (DM) and primitive mantle (PM) are respectively from Mckenzie and O'Nions (1991) and Sun and McDonough (1989). Garnet-lherzolite and spinel-lherzolite melting curves sources and the compositions of both DM and PM are from Aldanmaz et al. (2000). The E-MORB and N-MORB compositions are from Sun and McDonough (1989)

Tcheumenak Kouémo et al. 2014, 2023; Efon Awoum et al. 2020; Achu Megnemo et al. 2021; Sobzé Yemdji et al. 2023).

Geotectonic setting

In the Hf/3-Th-Ta from Wood (1980), amphibolites plot dominantly in VAB to MORB domains, which is consistent with oceanic crust. This oceanic crust also register active margin signature as evidence by the Fe_2O-MgO-Al_2O_3 diagram (Fig. 11e) from Pearce et al. (1977). This oceanic crust was certainly dragged towards a subduction trench and underwent contamination as evidenced by the Th/Yb = f(Nb/Yb) diagram from Sun and Mc Donough (1989) (Fig. 11f). This contamination involves both sediments and slab fluids as indicated by the Th/Yb vs Ba/La diagram (Fig. 11f). The slightly negative to positive anomaly displays by Ce/Ce* (Table 1) and Fig. 9b evidences the contamination by pelagic sediments (Fozing et al. 2019). The sediments that were dragged in the subduction trench finally led to the enrichment of these rocks in K, Rb Th and Ce (Fig. 9b) as well as various hydrothermal fluids during the subduction process. Indeed, the Ta-Nb and Ti negative anomalies displays by multi-element spider diagram (Fig. 9b) as well as active margin setting indicated by Fig. 11e are compatible with subduction setting and may thus evidenced the fact that amphibolites' protoliths underwent metamorphic transformation in this geotectonic environment. The subduction was followed by the collision, during the pan-African orogeny. This collision phenomenon is clearly evidenced in the field by strong occurrence of (i) granulite to eclogite facies metamorphic rocks represented by Grt-Ky-Sil gneiss (Tchaptchet

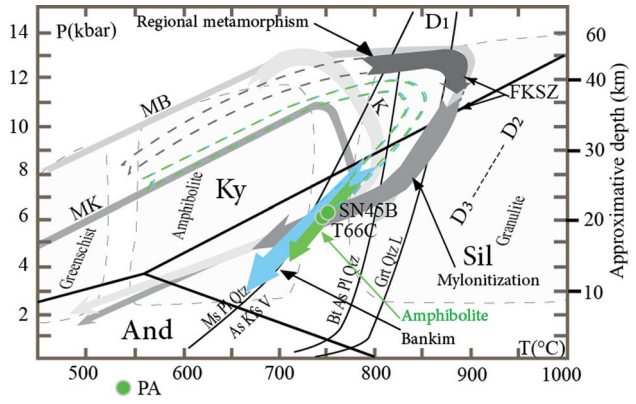

Fig. 12 Metamorphic *P–T-t* path of the Bankim amphibolites *P–T-t* path Alumino-silicate stability diagram is from Spear (1993). Facies domains and approximate depth are from Burcher and Rodney (2011). T66C: sample T66C**.** MK: Mayo Kout, MB: Mayo Banyo (Bouyo Houketchang et al. 2013). K: Kékem (Tchato et al. 2009). FKSZ: Fotouni-Kékem shear zone (Tcheumenak Kouémo et al. 2023). As: Alumino-silicate. L: Fluide. V: Gas. The Bankim *P–T* trajectory is after after Efon Awoum (2021)

Tchato et al. 2009; Bouyo Houkentchang et al. 2013; Tcheumenak Kouémo et al. 2014, 2023) and orthogneiss, displaying garnet amphibolites and pyroxene amphibolites (Fig. 4; Fozing et al. 2019; Ganwa 2005) and eclogite enclaves, (ii) calc-alkaline synkinematic plutons represented by I-types and S-types granites (Kwékam et al. 2010, 2015, 2020a, 2020b; Djouka-Fonkwé et al. 2008; Efon Awoum 2021Achu Megnemo, 2023).

P–T-t path evolution of amphibolites and geodynamic significance

Stable pyroxene crystals, the early to peak metamorphic stage-related microstructures are very scarce in the FKSZ and NMSZ certainly due to multi-phase deformations related collision and post collision processes. The few remnant of this specific structures and microstructure (Figs. 4c) are certainly related to the high-grade metamorphism peak phase. According to Passchier and Coelho (2006), Tcheumenak Kouémo et al. (2023) and Sobzé Yemdji et al. (2023) stable clinopyroxene displaying amphibole inclusion (Fig. 4j) that occurs in such a metamorphic rock indicate a granulite facies, while stable amphibole crystals indicate amphibolite facies. This is also supported by Pattison (2003) according to who, the occurrence of garnet and clinopyroxene (Fig. 4j–l) is symptomatic of granulite facies. Primary paragenesis for clinopyroxene amphibolites consists of stable amphibole + (metastable) clinopyroxene + plagioclase + K-feldspar, with quartz occurring as inclusions in amphibole. Boundaries granulation display by amphibole crystals (Fig. 4b), sharp and straight mineral boundaries displayed by plagioclase, pyroxene and amphibole (Fig. 4c), as well as pyroxene, amphibole and plagioclase showing triple points (Fig. 4c) and curved plagioclase twinning, characterize high grade amphibolite to low grade granulite metamorphic facies, whose *P–T* conditions are greater than 6 kb/750 °C (Fig. 12, Pons 2001; Passchier and Coelho 2006; Ten Grotenhuis et al. 2003; Bouyo Houkentchang et al. 2013; Bose et al. 2015; Efon Awoum et al. 2020; Tcheumenak Kouémo et al. 2023). The studied amphibolies occur in kyanite-sillimanite-garnet gneiss in both the FKSZ and NMSZ as well as in the Mayo Banyo located to the NE of the NMSZ, for which *P–T* conditions were estimated at 11.5–13.5 kbar/850–900 °C for the peak of the regional metamorphism (Bouyo Houkentchang et al. 2013; Tcheumenak Kouémo et al. 2023; Sobzé Yemdji et al. 2023). At such a high-grade metamorphism, garnet is expected in a mafic-granulite rock. This is evidenced in the field by mafic rock outcrop showing well-preserved garnet crystals in Bankim (Fig. 4k), in the Tikar Plain, located between the FKSZ and the NMSZ (Fig. 1). The peak metamorphism was attained in metapelites during the D_1 deformation at 600 Ma coeval to the continent–continent collision between the Saharan Metacraton and the Congo Craton (Fig. 1a, Bouyo Houkentchang et al. 2013; Tcheumenak Kouémo et al. 2023; Sobzé Yemdji et al. 2023). The metamorphism' peak was follow by retrograde phase, mainly preserved in the study areas as evidenced by pyroxene and garnet transformation respectively into amphibole and opaque minerals hornblende, plagioclase and opaque minerals (Fig. 4g, h, l). This retrograde metamorphism (Fig. 13b) seems to have been accompanied by contribution of hydrothermal fluids. The interaction between amphibolites and high temperature fluids during the retrograde metamorphic process is evidenced by hornblende replacing clinopyroxene (Fig. 4g, h) according to the reactional equation bellow:

Clinopyroxene + plagioclase + H_2O = hornblende + Op (Ilm) + quartz.

The above retromorphic transformation occurs around *P–T* condition around 6 kbar/750 °C according to Bouyo Houkentchang et al. 2013 and Tcheumenak Kouémo et al. (2023), evidencing decompression at high but approximately the same temperature (isothermal decompression, Tchaptchet Tchato et al. 2009, Bouyo Houkentchang et al. 2013; Tcheumenak Kouémo et al. 2023). This retromorphic paragenesis rather indicate a transitional than the highest P–T metamorphic grade underwent by the studied rocks. The approximately isothermal retrograde metamorphism was certainly related to relaxation during D_2-D_3 consecutive to the stress release and erosion-isostatic reequilibration processes that will have provided decompression (Fig. 13b) coeval to the post-collisional history of the Western Gondwana (Tchaptchet Tchato et al. 2009, Bouyo Houkentchang et al. 2013; Tcheumenak Kouémo et al. 2023).

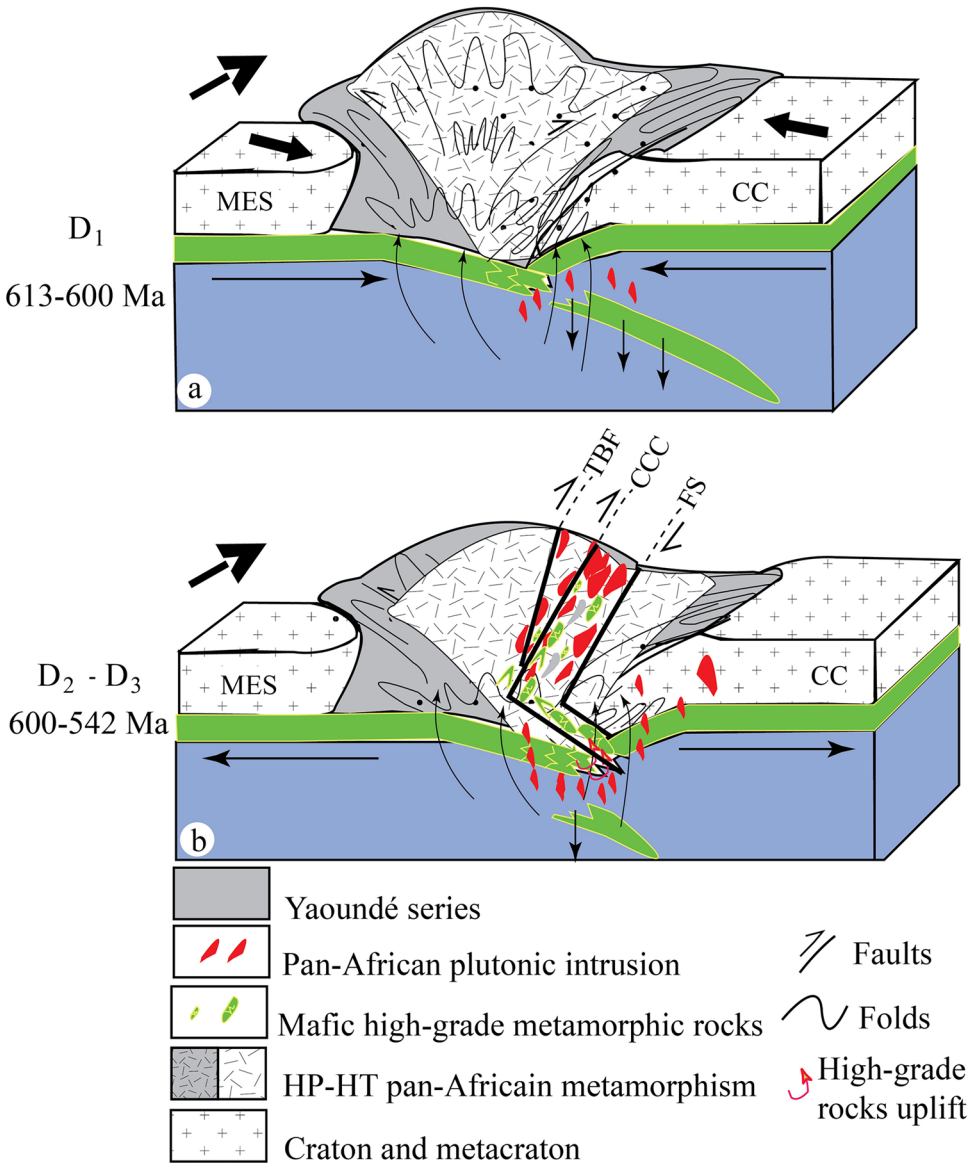

Fig. 13 Tectono-metamorphic evolution model of the Pan-African fold belt showing dismembered green rocks (amphibolites) and high-grade metamorphic rocks within the CCSZ and the SF

The regional metamorphism was overprinted by the early sinistral syn-D_2 and late dextral syn-D_3 shear deformation phases during the post-collisional history of the Western Gondwana leading to the formation mylonitic corridors along shear zones including the CCSZ (together with FKSZ and the NMSZ branches (Fig. 2) and the SF. Field evidences of these shear zones for example, are the NE-SW mylonitic corridors described from Kékem to Nyakong along the CCSZ (Njonfang et al. 2006, 2008; Tcheumenak Kouémo et al. 2023; Sobzé Yemdji et al. 2023). Fish-like (Fig. 5i) and lens-like (Fig. 4d) structures display by amphibole crystals indicate high P–T ductile deformation conditions characterizing high-grade amphibolite to low-grade granulite facies (Storey et al. 2001; Ten Grotenhuis et al. 2003; Passchier and Coelho 2006; Tcheumenak Kouémo et al. 2023; Sobzé Yemdji et al. 2023). The above data indicate that the mylonitization events occur at *P–T* conditions greater than 6 kbr/750 °C during the late to post-collisional history (D_2-D_3) of the Western Gondwana (Tcheumenak Kouémo et al. 2023; Sobzé Yemdji et al. 2023). The polyphasic activations of faults such as the CCSZ and SF (Fig. 13c) during D_2-D_3 phases, together with the emplacement of synkinematic plutons contributed in stretching, shearing, folding dismembering (Figs. 5b–i, 10b, c, 13b) and scattering metabasites (amphibolites) and metapelite (kyanite-sillimanite-garnet gneiss), along the Pan-African mobile zone during late phases (D_2-D_3) of the Pan-African orogeny as it is evidenced in the field (Figs. 2, 3, 13b).

Conclusion

Petrographic, microstructural, geochemical (whole-rock and Sr–Nd) data of amphibolites from FKSZ and NMSZ, were used to characterize their origin, *P–T-t* path evolution, to explain their shapes and distribution along the CCSZ, and their contribution for better understanding of geodynamic evolution of the CAFB during the Pan-African orogeny.

From a structural point of view, three deformation phases are recorded in these shear zones, from the oldest to the youngest, D_1, D_2 and D_3. The D_1 phase, is remnant and marked by a NW–SE S_1 foliation. The D_2 phase is sinistral shear phase, marked by NNW-SSE to NNE-SSW S_2 foliation, C_2 shear planes, B_2 shear band boudins, F_2 knee-like folds and lens-like and fish-like structures. The D_3 phase is a NE-SW dextral mylonitic shear phase, marked by S_3 foliation, C_3 shear planes, P_3 recumbent and overturn folds, B_3 shear band boudins and σ-type sigmoids.

From a petrographic point of view, PA occurs as slab stones, lenses to lens-like, egg-like enclaves, folded bands, sheared and/or boudinaged green to dark green, displaying NE-SW preferred orientation. It displays heterogranular nematoblastic texture consisting of hornblende, plagioclase and clinopyroxene porphyroblasts. Microscopic data indicate that PA underwent multi-phase deformations and polyphasic (prograde-peak-retrograde) high-grade granulite facies metamorphism during the collision and post collision processes, but only its retrograde phase is well preserved. This retrograde metamorphism was overprinted by D_2-D_3 mylonitic deformation during the late stage of the Pan-African orogeny history during which green rocks were stretched, sheared, folded, dismembered and scattered along the Pan-African mobile zone.

From a geochemical point of view, PA derives from a mafic protoliths that was contaminated by both subducted sediment and slab-derived fluids. The model age ($T_{DM} = 1.25$ Ga) with initial $^{87}Sr/^{86}Sr$ ratios of 0.70488 suggest an ancient Mesoproterozoic source material that underwent metamorphic transformation during the collisional (burial) and post collisional (exhumation) stapes of the Pan-African orogeny.

Acknowledgements Numerous laboratory results contained in this paper are part of petrographic, geochemical (whole-rock and isotopic) data obtained during a stay by Prof Kwékam Maurice in ''Geowissenschaftliches Zentrum Göttingen, Universität Göttingen", Germany financed by the Germany Academic Exchange Organisation (DAAD). The authors address their warmest thanks to Prof Gerald Wörner for providing facilities. Thoughtful reviews by anonymous reviewers significantly contributed to improve the original manuscript. These reviews are gratefully acknowledged.

Author contributions Tcheumenak Kouémo Jule, Sobze Yemdji Belmien Robinson Tepi Yemele Brice Rostant, and Azefack Mbounou Rodolph Loïque carried out field investigations, sample collection and preparation. Kwékam Maurice performed part of thin sections realization, Sr-Nd and part of the geochemical data analyses in the Geowissenschaftliches Zentrum Göttingen, Georg-August Universität, Abteilung Geochemie, Laboratory in Germany. The authors conceptualized the preliminary' paper ideas, presented the methodology, processed data using softwares, prepared the original draft, discussed the results and contributed for the final manuscript.

Data availability Raw data are available on request from the authors.

Declarations

Conflict of interest We, the authors declare that no known competing financial interests or personal relationships that could influence the publication of work presented in this paper.

References

Abdelsalam MG, Liégeois JP, Stern RJ (2002) The Sahara metacraton. J Afr Earth Sci 34:119–136

Achu Megnemo L, Kwékam M, Fozing EM, Tcheumenak Kouémo J, Efon Awoum J, Choumele Kana SC, Sobze Yemdji RB, Kamgang Tchuifong AB, Azemekeu Folefack L (2021) Field observations and microstructural evidences of syntectonic emplacement of the Ngwi granitic plutons (Central Cameroon domain). Arab J Geosci 14:1497

Aldanmaz E, Pearce JA, Thirlwall MF, Mitchell JG (2000) Petrogenetic evolution of the late Cenozoic, post-collision volcanism in western Anatolia, Turkey. Journal of Volcanology Geother Res 102:67–95

Bella Nké BE, Njanko T, Mamtani MA, Njonfang E, Rochette P (2018) Kinematic evolution of the Mbakop Pan-African granitoids (western Cameroon domain): An integrated AMS and EBSD approach. J Struct Geol 111:42–63

Bose S, Guha S, Ghosh G et al (2015) Tectonic Juxtaposition of crust and continental growth during orogenesis: example from the Rengali Province. Eastern India Geosci Frontiers 6(4):537–555. https://doi.org/10.1016/j.gsf.2014.09.002

Bouyo Houketchang M, Toteu SF, Deloule E, Penaye J, Van Schmus WR (2009) U-Pb and Sm-Nd dating of high-pressure granulites from Tcholliré and Banyo regions: Evidence for a Pan-African granulite facies metamorphism in north-central Cameroun. J Afr Earth Sci 54:144–154

Bouyo Houketchang M, Penaye J, Barbey P, Toteu SF, Wandji P (2013) Petrology of high-pressure granulite facies metapelites and metabasites from Tcholliré and Banyo regions: Geodynamic implication for the Central African Fold Belt (CAFB) of north-central Cameroon. Precambrian Res 224:12–433

Condie KC (1997) Sources of proterozoic mafic dyke Swarms: constraints from Th/Ta and La/Yb ratios. Precambrian Res 81:3–14

De La Roche H (1965) Sur l'existence de plusieurs facies geochimiques dans les schistes paleozoiques des pyrenees luchonnaises. Geol Rundsch 5:274–301

Djouka-Fonkwé ML, Schulz B, Schüssler U et al (2008) Geochemistry of the Bafoussam Pan-African I- and S-Type Granitoids in Western Cameroon. J Afr Earth Sci 50(2–4):148–167. https://doi.org/10.1016/j.jafrearsci.2007.09.015

Efon Awoum J, Fozing EM, Kwékam M, Tcheumenak Kouémo J, Choumele Kana SC, Achu Megnemo L (2020) Structural characterization of the Pan-African Ndiéki area in the Foumban-Bankim Shear Zone (West Cameroon): constraints from field observations and microstructures. Arab J Geosci 13:831

Efon Awoum J (2021) Pétrologie, structure et géochimie du massif de Ndiéki (Adamaoua-Cameroun). Doctorat/PhD Thesis, University of Dschang, 179p

Fozing EM, Mengou AC, Njanko T et al (2019) Emplacement of the Dschang Granitic Pluton (West-Cameroon): constraints from microstructures and magnetic fabrics. J Afr Earth Sc 156:144–157. https://doi.org/10.1016/j.jafrearsci.2019.05.007

Fozing EM, Kwékam M, Tcheumenak Kouémo J et al (2021) Kinematic Analysis of the Dschang Granitic Pluton (West-Cameroon): implications to the Pan-African deformation of the central african fold belt in cameroon during the post-collisional history of Western Gondwana. Precambr Res 359:106231. https://doi.org/10.1016/j.precamres.2021.106231

Frey FA, Garcia MO, Wise WS, Kennedy A, Gurriet P, Albarede F (1991) The evolution of Mauna Kea volcano, Hawaii: petrogenesis of tholeiitic and alkalic basalts. J Geophys Res 96:14347–14375

Ganwa AA (2005) Les granitoides de Méiganga : étude pétrographique, géochimique, structurale et géochronologique. Thèse d'État ès sciences naturelles université Yaoundé, Leur place dans la chaîne panafricaine, p 162p

Goldstein SL (1988) Decoupled evolution of Nd and Sr isotopes in the continental crust. Nature 336:733–738

Green NL (2006) Influence of slab thermal structure on basalt source regions and melting conditions: REE and HFSE constraints from the Garibaldi volcanic belt, northern Cascadia subduction system. Lithos 87:23–49

Hunter MA, Bickle MJ, Nisbet EG, Martin A, Chapman HJ (1998) Continental extension setting for the Archean Belingwe greenstone belt, Zimbabwe. Geol 26:883–886

Kamgang Tchuifong AB, Tcheumenak Kouémo J, Fozing EM, Achu Megnemo L, Efon Awoum J, Sobze BR, Safianou O, Kwékam M (2022) Geological mapping and structural interpretation of the Dschang-Santchou-escarpment (West, Cameroon), using Landsat 8 OLI/TIRS sensors/SRTM and field observations. Geol J. https://doi.org/10.1002/gj.4646

Kwékam M, Liégeois JP, Njonfang E, Affaton P, Hartmann G, Tchoua F (2010) Nature, origin and significance of the Fomopéa Pan-African high-K calc-alkaline plutonic complex in the Central African fold belt (Cameroon). J Afr Earth Sci 57:79–95

Kwékam M, Affaton P, Bruguier O, Liégeois JP, Hartmann G, Njonfang E (2013) The Pan-African Kekem gabbro-norite (West-Cameroon), U-Pb zircon age, geochemistry and Sr–Nd isotopes: geodynamical implication for the evolution of the Central African fold belt. J Afr Earth Sci 84:70–88

Kwékam M, Hartmann G, Njanko T, Tcheumenak Kouémo J, Fozing E, Njonfang E (2015) Geochemical and Isotope Sr-Nd Character of Dschang Biotite Granite: implications for the Pan-African continental crust evolution in West-Cameroon (Central Africa). Earth Sci Res 4:88–102

Kwékam M, Talla V, Fozing EM, Tcheumenak Kouémo J, Dunkl I, Njonfang E (2020b) The Pan-African high-K I-Type granites from Batié complex (West-Cameroon): age, origin and tectonic implications. Frontiers Earth Sci 8:363

Kwékam M, Dunkl I, Fozing EM, Hartmann G, Njanko T, Tcheumenak Kouémo J, Njonfang, E., (2020a). Syn-kinematic ferroan high-K I-type granites from Dschang in southwestern Cameroon: U-Pb age, geochemistry and implications for crustal growth in the late Pan-African orogeny. Geol Soc London, Spec Publ 502. https://doi.org/10.1144/SP502-2019-19

Liégeois JP, Abdelsalam MG, Ennih N, Ouabadi A (2013) Metacraton: nature, genesis and behavior. Gondwana Res 23:220–237

Le Maître RW, Bateman P, Dubek A, Keller J, Lameyre J, Le Bas MJ, Sabine PA, Schhmid R, Sorensen H, Streckeinsen A, Woolley AR Nzanettin B (1989) A classification of igneous rocks and glossary of terms. Recommendations of the International Union of Geological Sciences Subcommission on the Systematics of Igneous Rocks. Blackwell, Oxford, p 193

McDonough WF, Sun S-S (1995) The composition of the Earth. Chem Geol 120:228

McKenzie D, O'Nions RK (1991) Partial melt distribution from inversion of rare earth element concentrations. J Petrol 32:1021–1091

Ngako V, Affaton P, Nnanga JM, Njanko T (2003) Pan-African tectonic evolution in central and southern Cameroon: transpression and transtension during sinistral shear movements. J Afr Earth Sci 36:207–214

Ngako V, Affaton P, Njonfang E (2008) Pan-African tectonic in northwestern Cameroon: implication for history of Western Gondwana. Gondwana Res 14:509–522

Nguiessi Tchankam C, Nzenti JP, Nsifa NE, Tempier P, Tchoua F (1997) Les granitoïdes calco-alcalins, syn-cisaillement de Bandja dans la chaîne panafricaine nord-équatoriale au Cameroun. C R Acad Sci Paris 325:95–101

Njanko T, Nédélec A, Affaton P (2006) Synkinematic high-K cal akaline plutons associated with the Pan-African Central Cameroun shear zone (W-Tibati area): petrology and geodynamic significance. J Afr Earth Sci 44:494–510

Njanko T, Nédélec A, Kwékam M, Siqueira R, Esteban L (2010) Emplacement and deformation of the Fomopéa pluton: implication for the Pan-African history of Western Cameroon. J Struct Geol 32:306–320

Njanko T, Fozing EM, Kwekam M, Yakeu Sandjo AF, Njonfang E (2012) Magnetic characterization of Amphibolites from Fomopéa pluton (West Cameroon): their implication in the Pan-African deformation of Central African fold belt. Acta Geol Sinica 86:73–84

Njonfang E, Ngako V, Kwekam M et al (2006) Les Orthogneiss Calco-Alcalins de Foumban–Bankim: Témoins Dune Zone interne de marge active Panafricaine en Cisaillement. CR Geosci 338(9):606–616. https://doi.org/10.1016/j.crte.2006.03.016

Njonfang E, Ngako V, Moreau C et al (2008) Restraining bends in high temperature shear zones: the "Central Cameroon Shear Zone", Central Africa. J Afr Earth Sc 52(1/2):9–20. https://doi.org/10.1016/j.jafrearsci.2008.03.002

Ntieche B, Mohan MR, Amidou M (2017) Granitoids of the Magba Shear Zone, West Cameroon, Central Africa: evidences for emplacement under transpressive tectonic egime. J Geol Soc India 89(1):33–46. https://doi.org/10.1007/s12594-017-0556-4

Owona S, Mvondo Ondoa J, Ekodeck GE (2013) Evidence of quartz, feldspar and amphibole crystal plastic deformations in the Paleoproterozoic Nyong complex shear zones under amphibolite to granulite conditions (West Central African Fold Belt, SW Cameroon). J Geogr Geol 5(3):186–201

Passchier C, Coelho S (2006) An outline of shear-sens analysis in high-grade rocks. Gondwana Res 10:66–76

Pattison DRM (2003) Petrogenetic significance of orthopyroxene-free garnet+ clinopyroxene+ plagioclase±quartz-bearing metabasites with respect to the amphibolite and granulite facies. J Metamorphic Geol 21(1):21–34

Pearce JA (1983) Role of the sub-continental lithosphere in magma genesis at active continental margins. In: Hawkesworth CJ, Norry MJ (eds) Continental basalts and mantle xenoliths. Shiva Nantwich, pp 230–249

Pearce TH, Gorman BE, Birkett TC (1977) The relationship between major element chemistry and tectonic environment of basic and intermediate volcanic rocks. Earth Planet Sci Lett 36:121–132

Penaye J, Toteu SF, Van Schumus WR, Nzenti JP (1993) U-Pb and Sm-Nd Preliminary geologic data on the Yaoundé séries Cameroon. Reinterpretation of the Granulitic rocks as suture of

a collision in the "Central African" belt. C R Acad Sci Paris 317:789–794
Penaye J, Toteu SF, Tchameni R, Van Schumus WR, Tchakounté J, Ganwa A, Minyem D, Nsifa EN (2004) The 2.1 Ca West Central African belt in Cameroon: extension and evolution. J Afr Earth Sc 39:159–164
Pons JC (2001) La petro sans peine 2. Minéraux et roches métamorphiques. C.P.D.P. Acad Grenoble 228 p
Sobze Yemdji, B. R., Tcheumenak Kouémo, J., Fozing, E. M., Achu Megnemo L., Efon Awoum, J., Kamgang Tchuifong, A. B., Tepi Yemele, B. R., Kwékam, M., (2023). Kinematic evolution of the Nyakong-Manyi Shear Zone (Adamawa, Cameroon): constraints from field observations and microstructures, and implication for metamorphic P-T-t. Estimation. J Earth Sci 34(5):1465–1487 https://doi.org/10.1007/s12583-023-1816-4. http://en.earth-science.net
Spear FS (1993) Metamorphic phase equilibria and pressure-temperature-time paths. Monograph Series MSA, Washington DC, p 799
Storey CD, Prior DJ, Wheeler J (2001). Garnet crystal plasticity in an amphibolite facies shear zones: SEM-EBSD constraints on garnet deformation mechanisms and implication for UHPM terrain. UHPM Workshop, Waseda Univ 3B07:101–105
Sun SS, McDonough WF (1989) Chemical and isotopic systematics of oceanic basalts: implications for mantle composition and processes. In: Saunders AD, Norry MJ (eds) Magmatism in Ocean Basins. Spec Publ, Geol Soc London, pp 313–345
Tagne-Kamga G, Mercier E, Rossy M, Nsifa EN (1999) Synkinematic emplacement of the Pan-African Ngondo igneous complex (West Cameroon, central Africa). J Afr Earth Sci 28:675–691
Tchaptchet Tchato D, Schulz B, Nzenti JP (2009) Electron microprobe dating and thermobarometry of Neoproterozoic metamorphic events in the Kékem area, Central African Fold Belt of Cameroon. Stuttgard 186:95–109
Tcheumenak KJ, Njanko T, Kwékam M, Naba S, Bella Nke BE, Yakeu Sandjo AF, Fozing EM, Njonfang E (2014) Kinematic evolution of the Fodjomekwet-Fotouni shear zone: Implication for emplacement of the Fomopéa and Bandja plutons. J Afr Earth Sci 99:261–275
Tcheumenak KJ, Fozing EM, Zagalo AH, Noudiédié Kamgang JA, Kwékam M, Njonfang E (2023) Structural and petrographic characterization of the Fotouni-Kekem Shear Zone: implication for *P-T-t* regional metamorphism and Mylonitic Evolutions along the Central Cameroon Shear Zone. Arab J Geosci 14:1497. https://doi.org/10.1007/s12517-022-11095-1
Ten Grotenhuis SM, Trouw RAJ, Passchier CW (2003) Evolution of mica fish in mylonitic rocks. Tectonophysics 372:1–21
Toteu SF, Van Schmus RW, Penaye J, Michard A (2001) New U-Pb and Sm-Nd data from North-Central Cameroon and its bearing on the Pre-Pan-African history of Central Africa. Precambrian Res 108:45–73
Toteu SF, Penaye J, Poudjom Djomani Y (2004) Geodynamic evolution of Pan-African belt in central Africa with special reference to Cameroun. Candian J Earth Sci 41:73–85
Walker KR, Joplin GA, Lovering JF (1959) Metamorphic and metasomatic convergence of basic igneous rocks and lime-magnesia sediments of the precambrian of North-Western Queensland. J Geol Soc Australia 6(2):149–177
Wood DA (1980) The application of a Th-Hf-Ta diagram to problems of tectono-magmatic classification and to establishing the nature of crustal contamination of basaltic Lavas of the British tertiary volcanic province. Earth Planet Sci Lett 50:11–30